

Capacity Gains in MIMO Systems with Few-Bit ADCs Using Nonlinear Analog Operators

Marian Temprana Alonso[†], Xuyang Liu[‡], Farhad Shirani^{*†}, Hamidreza Aghasi[‡]

[†] Florida International University, [‡] University of California, Irvine,

Email: {mtemp009,fshirani}@fiu.edu, {xuyanl3,haghasi},@uci.edu

Abstract

Analog to Digital Converters (ADCs) are a major contributor to the power consumption of multiple-input multiple-output (MIMO) receivers with large antenna arrays operating in the millimeter wave and terahertz carrier frequencies. This is especially the case in large bandwidth terahertz communication systems, due to the sudden drop in energy-efficiency of ADCs as the sampling rate is increased above 100MHz. Two mitigating energy-efficient approaches which have received significant recent interest are i) to reduce the number of ADCs via analog and hybrid beamforming architectures, and ii) to reduce the resolution of the ADCs which in turn decreases power consumption. However, decreasing the number and resolution of ADCs leads to performance loss — in terms of achievable rates — due to increased quantization error. In this work, we study the application of practically implementable nonlinear analog operators such as envelop detectors and polynomial operators, prior to sampling and quantization at the ADCs, as a way to mitigate the aforementioned rate-loss. A receiver architecture consisting of linear analog combiners, nonlinear analog operators, and few-bit ADCs is designed. The fundamental information theoretic performance limits of the resulting communication system, in terms of achievable rates, are investigated under various assumptions on the set of implementable analog operators. Various numerical evaluations and simulations of the communication system are provided to compare the set of achievable rates under different architecture designs and parameters. Circuit simulations in a 65 nm CMOS technology exhibiting the generation of envelope detectors and polynomial operators are provided, and their power consumption is compared.

This work was presented in part at 2022 IEEE International Symposium on Information Theory [1], and 2022 IEEE Global Communications Conference [2]. This work was supported in part by NSF grant CCF-2241057.

**Corresponding Author: Farhad Shirani, Email: fshirani@fiu.edu*

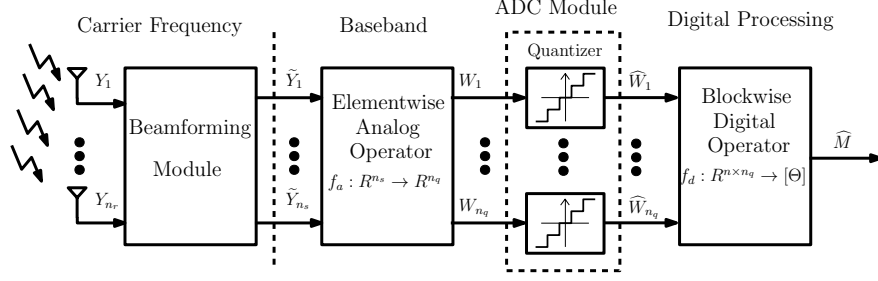


Fig. 1: The receiver architecture consists of an analog/hybrid beamforming module, an elementwise analog operator $f_a(\cdot)$, n_q low-resolution ADCs, and a blockwise digital operator $f_d(\cdot)$ with blocklength n . Y represents the received signal, \hat{M} is the message reconstruction, and $[\Theta]$ is the message set.

I. INTRODUCTION

In order to accommodate the ever-growing demand for higher data-rates, the wireless spectrum has been continuously expanding over the past several decades. Millimeter wave (mm-wave) communication networks are already being used in the fifth generation (5G) wireless systems to allow for larger channel bandwidths compared to earlier generation radio frequency (RF) systems which operate in frequencies below 6 GHz [3]. In pursuing this relentless trend towards achieving higher data rates using larger channel bandwidths, attention is shifting to the next frontier, which is to utilize the terahertz (THz) frequency bands, broadly defined as 0.1–10 THz [4]–[6]. This paradigm is being facilitated by recent advances in the design of integrated circuits and systems and antenna elements operating at THz frequencies. [7]–[12] The energy consumption of components such as analog to digital converters (ADCs) increases significantly in mm-wave and THz systems due to several factors as elaborated in the following. In theory, the power consumption of an ADC grows linearly with bandwidth, and the rate of increase is even more significant in practical implementations due to the excessive loss associated with the passive components at higher frequencies which causes an abrupt drop in ADC energy-efficiency as the bandwidth is pushed past 100 MHz [6], [13]–[15]. For instance, the power consumption of current commercial high-speed (≥ 20 GSamples/s), high-resolution (e.g. 8-12 bits) ADCs is around 500 mW per ADC [16]. Furthermore, in order to mitigate the inherent high isotropic path loss and sensitivity to blockages at high frequencies mm-wave and THz systems must leverage directive narrow-beams, by using large antenna arrays to increase the antenna gain at both base stations (BS) and user-ends (UE) [4]–[6], [17]. For instance, 5G wireless networks envision hundreds of antennas at the BS and in excess of ten antennas at the UE [18], and in THz application scenarios antenna arrays with hundreds of elements are being considered [19], [20]. In conventional multiple-input multiple-output (MIMO) systems with digital beamforming,

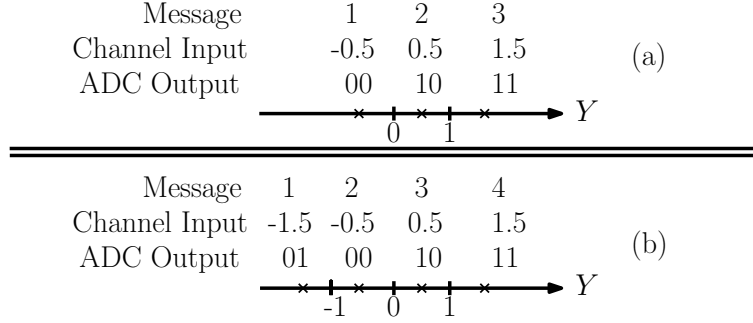


Fig. 2:(a) $X \in \{-0.5, 0.5, 1.5\}$ and the ADCs generate $Y \leq 0$ and $Y \leq 1$, and (b) $X \in \{-1.5, -0.5, 0.5, 1.5\}$, and the two ADCs generate $Y \leq 0$ and $|Y| \leq 1$.

each antenna output is digitized separately by a dedicated ADCs [21]. This requires a large number of ADCs which are a significant source of power consumption in large bandwidth MIMO receivers [22], [23]. Analog and hybrid beamforming has been proposed as a way to mitigate ADC power consumption by reducing the number of ADCs. Under hybrid beamforming, the receiver terminals use a collection of analog beamformers to linearly combine the large number of received signals and feed them to a small set of ADCs. Additionally, in standard ADC design, power consumption is proportional to the number of quantization bins and hence grows exponentially in the number of output bits [24] which prohibits the use of high resolution ADCs. There has been extensive recent efforts to design receiver architectures and coding strategies using analog and hybrid beamforming with a small number of few-bit ADCs [20], [22], [25]–[36].

In this work, we consider the use of nonlinear analog operators as a way to mitigate the rate-loss due to coarse quantization and increase channel capacity of MIMO systems with few-bit ADCs. To explain the aforementioned rate gains, let us consider a simple single-input single-output (SISO) scenario operating in the high signal-to-noise ratio (SNR) regime, i.e. $Y \approx X$. Assume that the receiver is equipped with two one-bit threshold ADCs. Then, as shown in Figure 2(a), it can receive at most three different messages per channel-use by performing two threshold comparisons, e.g. comparisons with threshold zero $Y \leq 0$ and threshold one $Y \leq 1$, hence achieving a rate of $R = \log 3$ bits/channel-use. Alternatively, if the receiver can produce the absolute value of the amplitude of the received analog signal, $|Y|$, then it can use the two comparators $Y \leq 0$ and $|Y| \leq 1$ as shown in Figure 2(b) to achieve $R = 2$ bits/channel-use, hence improving performance. The absolute value of the amplitude of the analog signal can be produced using envelope detectors. As an alternative approach, one could use polynomial analog operators, whose circuit implementation is studied in Section VI, instead of envelope detectors to replace $|Y|$ by Y^2 in the above construction. As discussed in this paper, design and implementation of envelope detectors is

simpler and more power efficient, whereas receiver architectures using polynomial analog operators may achieve higher communication rates especially in MIMO scenarios with large number of received signals.

The example described in Figure 2 serves as proof of concept that one can potentially reduce the rate-loss due to coarse quantization via non-linear analog processing. In the sequel, we will study the design of receiver architectures utilizing several classes of non-linear analog operators, their associated circuit designs, coding strategies, and the resulting channel capacities. To elaborate, we consider the general receiver model shown in Figure 1. The receiver operation is decomposed into analog processing, ADC, and digital processing modules. At each channel use, the channel output vector $Y^{n_r} = (Y_1, Y_2, \dots, Y_{n_r})$ is received, where n_r is the number of receiver antennas. The vector Y^{n_r} is passed through an analog/hybrid beamforming module which produces the vector \tilde{Y}^{n_s} , where $n_s = 1$ if analog beamforming is used and $n_s > 1$ if hybrid beamforming is used. \tilde{Y}^{n_s} is fed to an analog processing module $f_a(\cdot)$ to produce W^{n_q} , where n_q is the number of ADCs. The choice of the analog processing function $f_a(\cdot)$ is restricted due to the practical limitations in analog hardware design. In general, the analog function $f_a(\cdot)$ is chosen from a predefined set of implementable functions \mathcal{F}_a . The output of the analog processing module is fed to the ADCs, and the resulting sequence \widehat{W}^{n_q} is given to the digital processing module which operates *jointly* on the received block of output vectors over n channel-uses to reconstruct the transmitted message. In Section II, we consider the scenario where \mathcal{F}_a consists of analog processing functions generated by collections of envelope detectors, and propose receiver architectures, design coding strategies, derive the fundamental performance limits in terms of achievable rates. In Section III, we study receiver architectures, circuit design, and coding strategies associated with analog polynomial operators. Transceiver Circuit designs and simulations evaluating the power consumption of the nonlinear processing operators including sequences of concatenated envelope detectors and polynomial operators are provided in Section VI. Table I includes the design specifications of our proposed proof-of-concept THz transceiver to achieve data rates above 100 Gbps. In this instance, we adopt a 64-QAM modulation scheme across a 34 GHz bandwidth centered at the 120GHz carrier frequency to support a 100+ GbpS data rate. These specifications are comparable with recent implementations of transmitter circuit and antenna designs at this frequency range [9], [12], [37].

In summary, our main contributions are as follows:

- To characterize the channel capacity under analog beamforming when envelope detectors are used for analog signal processing. The capacity expression is derived in terms of the number of ADCs, n_q , number of output levels of each ADC, ℓ , and number of concatenated envelope detectors, δ_{env} (Theorems 1-3).
- To characterize the high SNR capacity under analog beamforming when polynomial operators are used

TABLE I: System Design Parameters of an instance of the proposed THz communication system achieving a 100+ Gbps bit rate.

Modulation	RF-64QAM
Baud Rate (Gbaud)	17
Bit Rate (Gbps)	102
Carrier Frequency (GHz)	120
RF Bandwidth (GHz)	34
Wireless Distance (m)	1
Path Loss (dB)	74.02
TX Antenna Array Gain (dBi)	25
RX Antenna Array Gain (dBi)	25
Transmitted Power (dBm)	5
Receiver Noise Figure (dB)	15
Receiver Signal Power (dBm)	-19
Receiver Sensitivity (dBm)	-28.7
Signal-to-Noise Ratio (dB)	25
Bit-Error-Rate	10^{-4}

for analog signal processing. The high SNR capacity and inner-bounds to the low SNR achievable rates are provided in terms of the number of ADCs, n_q , number of output levels of each ADC, ℓ , and the polynomial degree, δ_{poly} (Theorem 4).

- To provide a receiver architecture for hybrid beamforming using envelope detectors for ultra high data rate communication with QAM demodulation (Theorem 5).
- To provide computational methods for finding the set of achievable rates and quantifying the gains due to nonlinear analog processing under the proposed analog and hybrid beamforming architectures, and to provide explanations of how these gains change as SNR, n_q , ℓ , and δ are changed.
- To provide circuit designs and associated performance simulations for implementing polynomials of degree up to four and concatenated envelope detector sequences with a pair of envelope detectors; and to evaluate their power consumption.

Notation: The set $\{1, 2, \dots, n\}, n \in \mathbb{N}$ is represented by $[n]$. The vector (x_1, x_2, \dots, x_n) is written as $x(1:n)$ and x^n , interchangeably, and $(x_k, x_{k+1}, \dots, x_n)$ is denoted by $x(k : n)$. The i th element is written as $x(i)$ and x_i , interchangeably. We write $\|\cdot\|_2$ to denote the L_2 -norm. An $n \times m$ matrix is written as $h(1:n, 1:m) = [h_{i,j}]_{i,j \in [n] \times [m]}$, its i th column is $h(:, i), i \in [m]$, and its j th row is $h(j, :), j \in [m]$. We write \mathbf{x} and \mathbf{h} instead of $x(1:n)$ and $h(1:n, 1:m)$, respectively, when the dimension is clear from context. The

notation \mathbf{x}^H is used to denote the hermitian of \mathbf{x} . Sets are denoted by calligraphic letters such as \mathcal{X} , families of sets by sans-serif letters such as \mathbf{X} , and collections of families of sets by \mathcal{X} .

II. ANALOG BEAMFORMING ARCHITECTURE WITH ENVELOPE DETECTORS

In this section, we consider a MIMO receiver with analog beamforming equipped with a collection of envelope detectors for analog signal processing and a set of n_q few-bit ADCs. Analog beamforming utilizes analog phase shifters and only one RF chain for the beamforming operation [20], [38]. This leads to a simplified design and low power consumption compared to hybrid and digital beamforming. However, analog beamforming can only support single-stream transmission which yields lower data rates. The low power consumption makes analog beamforming suitable for long-distance transmission in THz applications [38]. Envelope detectors are suitable for analog processing of signals at high frequencies due to their low power consumption and simple circuit design [39]. This is particularly the case for THz communication, where compared to analog polynomial operators studied in [1], [2], the power consumption of envelop detectors is significantly lower at high data rates (see Section VI). An envelope detector is parametrized by its threshold $a \in \mathbb{R}$ and its operations on an input $x \in \mathbb{R}$ is captured by the function $A_1(x, a) = |x - a|$, $x \in \mathbb{R}$. Envelope detectors can be concatenated in a sequence to generate a larger collection of analog operators. The operation of a sequence of $s \in \mathbb{N}$ envelop detectors with bias vector $a^s = (a_1, a_2, \dots, a_s)$ is captured by the iterative relation $A_s(x, a^s) = |A_{s-1}(x, a^{s-1}) - a_s|$, $s > 1$. The concatenated envelope detector implementation developed in Section VI exhibits substantial power saving in THz communication systems compared to other possible approaches to mitigate the rate-loss due to coarse quantization, such as the approach of incorporating pipeline ADC architectures to perform beamforming [40]–[42]. This major power saving is achieved by removing the digital-to-analog converters (DAC) and the subtractors inside a pipeline ADC which are also very challenging to design at higher data rates. It should be noted that concatenating large numbers of envelop detectors leads to increased circuit noise, and power consumption. Hence, there is a tradeoff between power-consumption, circuit complexity and robustness, and degrees of freedom in generating analog processing functions which in turn affects the set of achievable rates. This tradeoff is quantified in this section by deriving the set of achievable rates in terms of the number of concatenated envelope detectors.

A. System Model

We consider a MIMO channel, whose input and output¹ $(\mathbf{X}, \mathbf{Y}) \in \mathbb{R}^{n_t \times n_r}$ are related through $\mathbf{Y} = \mathbf{h}\mathbf{f}\mathbf{X} + \mathbf{N}$, where $\mathbf{f} \in \mathbb{R}^{n_t \times 1}$ is the transmitter's beamforming vector with $\|\mathbf{f}\|_2 = 1$, $\mathbf{h} \in \mathbb{R}^{n_r \times n_t}$ is the (fixed) channel matrix, and \mathbf{N} is a jointly Gaussian noise vector. To perform analog beamforming, the receiver chooses a combining vector $\mathbf{w} \in \mathbb{R}^{n_r \times 1}$, where $\|\mathbf{w}\|_2 = 1$ and produces $Y \triangleq \mathbf{w}^H \mathbf{Y}$. To simplify the notation, we define $h \triangleq \mathbf{w}^H \mathbf{h}$, $X \triangleq \mathbf{f}^H \mathbf{X}$ and $N \triangleq \mathbf{w}^H \mathbf{N}$ and write $Y = hX + N$ as the resulting SISO channel. Without loss of generality, we assume that $N \sim \mathcal{N}(0, 1)$ and that the channel input has average power constraint P , i.e. $\mathbb{E}(X^2) \leq P$. In the model captured by Figure 1 and explained in the introduction, the choice of the decoding function at the receiver is restricted by the limitations on the number of low-resolution threshold ADCs, $n_q \in \mathbb{N}$, the number of output levels of the ADCs, $\ell \in \mathbb{N}$, and the set of *implementable nonlinear analog functions*. In this section, we consider using concatenated sequences of envelop detectors for analog signal processing. So, the set of implementable nonlinear analog functions is:

$$\mathcal{F}_{env}^\delta = \{f(y) = A_s(y, a^s), y \in \mathbb{R} | s \in [\delta], a^s \in \mathbb{R}^s\}, \quad \delta \in \mathbb{N},$$

where $A_1(y, a) \triangleq |y - a|$, $y, a \in \mathbb{R}$ and $A_s(y, a^s) \triangleq A_1(A_{s-1}(y, a^{s-1}), a_s) = |A_{s-1}(y, a^{s-1}) - a_s|$, $s \in \mathbb{N}$. That is, \mathcal{F}_{env}^δ consists of all functions which can be generated using sequences of $s \leq \delta$ concatenated envelop detectors with thresholds a_1, a_2, \dots, a_s , respectively. The restriction to a limited number of envelop detectors is due to limitations in analog circuit design, and the implementability of such functions is justified by the circuit designs and simulations provided in Section VI. Formally, the receiver (Figure 1), consists of:

- i) An analog beamforming module characterized by \mathbf{w} which takes \mathbf{Y} as input and outputs $Y = \mathbf{w}^H \mathbf{Y}$ using an analog power combiner (e.g., collection of phase shifters).
- i) A set of elementwise analog processing functions $f_j \in \mathcal{F}_{env}^\delta$, $j \in [n_q]$, $\delta \in \mathbb{N}$ operating on the beamformer output Y to produce the vector $W(1 : n_q)$, where $W(j) = f_j(Y)$, $j \in [n_q]$.
- ii) A set of n_q ADCs, each with ℓ output levels and threshold vectors $t(j, 1 : \ell - 1) \in \mathbb{R}^{\ell-1}$, $j \in [n_q]$ operating on the vector $W(1 : n_q)$ and producing $\widehat{W}(1 : n_q)$, where

$$\widehat{W}(j) = k \quad \text{if} \quad W(j) \in [t(j, k), t(j, k + 1)], k \in [0, \ell - 1],$$

¹To simplify notation, we have considered real-valued variables. The derivations can be extended to complex variables in a straightforward manner.

where $j \in [n_q]$ and we have defined $t(j, 0) \triangleq -\infty$ and $t(j, \ell) \triangleq \infty$. We call $t(1:n_q, 1:\ell-1)$ the *threshold matrix*. It is assumed that $0 < t(i, j) < t(i, j'), i \in [n_q], j, j' \in [\ell-1], j < j'^2$.

iii) A digital processing module represented by $f_d : \{0, 1, \dots, \ell-1\}^{n \times n_q} \rightarrow [\Theta]$, operating on the block of ADC outputs after n -channel uses $\widehat{W}(1:n, 1:n_q)$. After the n th channel-use, the digital processing module produces the message reconstruction $\widehat{M} = f_d(\widehat{W}(1:n, 1:n_q))$. The communication system is characterized by $(P, h, n_q, \delta, \ell)$, and the transmission system by $(n, \Theta, e, f^{n_q}, t(1:n_q, 1:\ell-1), f_d)$, where $f^{n_q} = (f_1, f_2, \dots, f_{n_q})$ and $f_j \in \mathcal{F}_{env}^\delta, j \in [n_q]$, and $e(\cdot)$ is such that the channel input satisfies the average power constraint. Achievability and probability of error are defined in the standard sense. The capacity maximized over all implementable analog functions using sequences of envelop detectors is denoted by $C_{env}(P, h, n_q, \delta, \ell)$.

B. Communication Strategies and Achievable Rates

In this section, we investigate the channel capacity for a given communication system parametrized by $(P, \mathbf{h}, n_q, \delta, \ell)$.

1) *Preliminaries:* We first introduce some useful terminology and preliminary results which will be used in the derivations throughout the rest of the paper. The quantization process at the receiver is modeled by two sets of functions. The analog processing functions $f_j(\cdot), j \in [n_q]$ and ADC threshold matrix $\mathbf{t} \in \mathbb{R}^{n_q \times (\ell-1)}$.

Definition 1 (Quantizer). Given a threshold matrix $\mathbf{t} \in \mathbb{R}^{n_q \times (\ell-1)}$ and a collection of functions $f_j \in \mathcal{F}_{env}^\delta$, a quantizer $Q : \mathbb{R} \rightarrow [\ell]^{n_q}$ characterized by the tuple $(\ell, \delta, n_q, f^{n_q}, \mathbf{t})$ is defined as $Q(\cdot) \triangleq (Q_1(\cdot), Q_2(\cdot), \dots, Q_{n_q}(\cdot))$, where $Q_j(y) \triangleq k$ iff $f_j(y) \in [t(j, k), t(j, k+1)], j \in [n_q]$. The associated partition of $Q(\cdot)$ is:

$$\mathbf{P} = \{\mathcal{P}_{\mathbf{i}}, \mathbf{i} \in [\ell]^{n_q}\} - \Phi, \text{ where } \mathcal{P}_{\mathbf{i}} = \{y \in \mathbb{R} | Q(y) = \mathbf{i}\}, \mathbf{i} \in [\ell]^{n_q}.$$

For a quantizer $Q(\cdot)$, we call $y \in \mathbb{R}$ a *point of transition* if the value of $Q(\cdot)$ changes at input y , i.e. if it is a point of discontinuity of $Q(\cdot)$. Let r be a point of transition of $Q(\cdot)$. Then, there must exist output vectors $\mathbf{c} \neq \mathbf{c}'$ and $\epsilon > 0$ such that $Q(y) = \mathbf{c}, y \in (r - \epsilon, r)$ and $Q(y) = \mathbf{c}', y \in (r, r + \epsilon)$. So, there exists $j \in [n_q]$ and $k \in [\ell-1]$ such that $f_j(y) < t(j, k), y \in (r - \epsilon, r)$ and $f_j(y) \geq t(j, k), y \in (r, r + \epsilon)$, or vice versa; so that r is a root of the function $f_{j,k}(y) \triangleq f_j(y) - t(j, k)$. Let $r_1, r_2, \dots, r_\gamma$ be the sequence of roots of $f_{j,k}(\cdot), j \in [n_q], k \in [\ell-1]$ (including repeated roots), written in non-decreasing order, where $\gamma \triangleq (\ell-1)n_q 2^\delta$.

²Note that the assumption $0 < t(i, j)$ does not loose generality since $0 \leq |y|, \forall y \in \mathbb{R}$. Hence, a negative threshold would yield trivial ADC output.

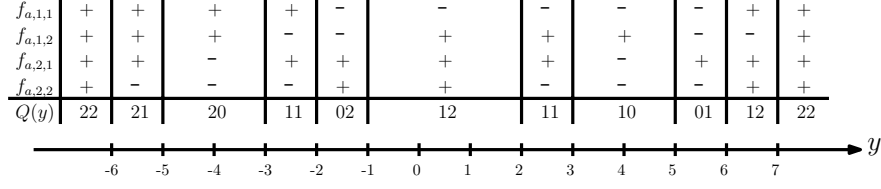


Fig. 3: The quantizer outputs in Example 1. The first four rows show the sign of the function $f_{j,k}$, $j, k \in \{1, 2\}$ for the values of y within each interval. The last row shows the quantizer output in that interval.

Let $C = (\mathbf{c}_0, \mathbf{c}_1, \dots, \mathbf{c}_\gamma)$ be the corresponding quantizer outputs, i.e. $\mathbf{c}_{i-1} = \lim_{y \rightarrow r_i^-} Q(y)$, $i \in [\gamma]$ and $\mathbf{c}_\gamma = \lim_{y \rightarrow \infty} Q(y)$. We call C the *code* associated with the quantizer and it plays an important role in the analysis provided in the sequel. Note that the associated code is an ordered set of vectors. The size of the code $|C|$ is defined as the number of unique vectors in C . Each $\mathbf{c}_i = (c_{i,1}, c_{i,2}, \dots, c_{i,n_q})$, $i \in \{0, 1, \dots, \gamma\}$ is called a codeword. For a fixed $j \in [n_q]$, the transition count of position j is the number of codeword indices where the value of the j th element changes, and it is denoted by κ_j , i.e., $\kappa_j \triangleq \sum_{k=1}^{\gamma} \mathbb{1}(c_{i_k-1,j} \neq c_{i_k,j})$. It is straightforward to see that $|\mathbf{P}| = |C|$ since both cardinalities are equal to the number of unique outputs the quantizer produces. The following example clarifies the definitions given above.

Example 1 (Associated Code). Let $n_q = \delta = 2$ and $\ell = 3$ and consider a quantizer characterized by analog processing functions $f_1(y) = A_2(y, (2, 4)) = \|y - 2\| - 4$ and $f_2(y) = A_2(y, (4, 0)) = \|y\| - 4$, $y \in \mathbb{R}$, and thresholds

$$t(1, 1) = 0, \quad t(1, 2) = 1, \quad t(2, 1) = 1, \quad t(2, 2) = 2,$$

We have:

$$f_{1,1}(y) = \|y - 2\| - 4 - 1, \quad f_{1,2}(y) = \|y - 2\| - 4$$

$$f_{2,1}(y) = \|y\| - 4 - 1, \quad f_{2,2}(y) = \|y\| - 4 - 2.$$

The ordered root sequence is $(r_1, r_2, \dots, r_{10}) = (-6, -5, -3, -2, -1, 2, 3, 5, 6, 7)$. The associated partition is:

$$\mathbf{P} = \{[-\infty, -6), (-6, -5), (-5, -3), (-3, -2), (-2, -1), (-1, 2), (2, 3), (3, 5), (5, 6), (6, 7), (7, \infty)\}.$$

The associated code is given by 22, 21, 20, 11, 02, 12, 11, 10, 01, 12, 22. This is shown in Figure 3. The size of the code is $|C| = 8$. The high SNR capacity of a channel using this quantizer at the receiver is $\log |\mathbf{P}| = \log |C| = \log 8$.

2) *Single Envelope Detector and One-bit Quantization*: As a first step, we investigate scenarios with $\ell = 2$ and $\delta = 1$. We will build upon this to derive capacity expressions for $\delta, \ell \in \mathbb{N}$. It can be noted that since $\delta = 1$, each $f_j(y)$ is of the form $|y - a_j|$ for some $a_j \in \mathbb{R}$. We sometimes write $f_{a_j,j}(y) = |y - a_j|$ to explicitly denote the value of a_j . Given threshold $t_j > 0$ the roots of $f_{a_j,j}(y) - t_j$ are equal to $a_j \pm t_j$. The following proposition provides the high SNR capacity when $\ell = 2, \delta = 1$.

Proposition 1. *Let $h \in \mathbb{R}$ and $n_q > 1$. Then,*

$$\lim_{P \rightarrow \infty} C_{\text{env}}(P, h, n_q, 2, 1) = 1 + \log n_q.$$

Proof. For a given quantizer, the high SNR achievable rate is equal to $\log |\mathbf{P}| = \log |\mathbf{C}|$. So, finding the capacity is equivalent to finding the maximum $|\mathbf{C}|$ over all choices of $Q(\cdot)$. First, let us prove the converse result. Note that $|\mathbf{C}| \leq 2n_q$ since $\mathbf{c}_0 = \mathbf{c}_{2n_q}$. The reason is that for the absolute value function $f_{a_j,j}(\cdot), j \in [n_q]$, we have $\lim_{y \rightarrow \infty} f_{a_j,j}(y) = \lim_{y \rightarrow -\infty} f_{a_j,j}(y) = \infty$. So,

$$c_{0,j} = \lim_{y \rightarrow -\infty} \mathbb{1}(f_{a_j,j} - t_j > 0) = \lim_{y \rightarrow \infty} \mathbb{1}(f_{a_j,j} - t_j > 0) = c_{2n_q,j}. \quad (1)$$

As a result, $\log |\mathbf{C}| \leq 1 + \log n_q$. Next, we prove achievability. Let $t_j = \frac{n_q+1}{2}, j \in [n_q]$ and $f_{a_j,j}(y) \triangleq |y - j - \frac{n_q+1}{2}|, j \in [n_q]$, so that the roots of $f_{a_j,j}(\cdot) - t_j$ are j and $j - n_q - 1$. Then, $(r_1, r_2, \dots, r_{2n_q}) = (-n_q, -n_q+1, \dots, -1, 1, 2, \dots, n_q)$ and

$$c(i, j) = \begin{cases} 1 - \mathbb{1}(j \leq i) & \text{if } i \leq n_q, \\ \mathbb{1}(n_q - j + 1 \leq i - n_q) & \text{otherwise.} \end{cases}$$

For instance for $n_q = 3$, we have $\mathbf{C} = (111, 011, 001, 000, 001, 011, 111)$. Hence, the only repeated codewords are \mathbf{c}_0 and \mathbf{c}_{2n_q} . As a result, $|\mathbf{C}| = 2n_q$, and $\log |\mathbf{C}| = 1 + \log n_q$ is achievable. \square

The following theorem provides a computable expression for the capacity under general assumptions on channel SNR.

Theorem 1. *Consider a system parametrized by $(P, h, n_q, \delta, \ell)$, where $P > 0, h \in \mathbb{R}, n_q > 1$, and $\delta = 1, \ell = 2$. Then, the capacity is given by:*

$$C_{\text{env}}(P, h, n_q, \delta, \ell) = \sup_{\mathbf{x} \in \mathbb{R}^{2n_q+1}} \sup_{P_X \in \mathcal{P}_{\mathbf{x}}(P)} \sup_{\mathbf{t} \in \mathbb{R}^{2n_q}} I(X; \widehat{Y}), \quad (2)$$

where $\widehat{Y} = Q(hX+N)$, $N \sim \mathcal{N}(0, 1)$, $\mathcal{P}_{\mathbf{x}}(P)$ is the set of probability distributions defined on $\{x_1, x_2, \dots, x_{2n_q+1}\}$ such that $\mathbb{E}(X^2) \leq P$, and $Q(y) = k$ if $y \in [t_k, t_{k+1}]$, $k \in \{1, \dots, 2n_q\}$ and $Q(y) = 0$ if $y > t_{2n_q}$ or $y < t_1$.

Proof. We provide an outline of the proof. First, we argue that the input alphabet has at most $2n_q + 1$ mass points since based on the proof of Proposition 1, the channel output can take at most $2n_q$ values.

Let the quantized channel output be denoted by \widehat{Y} . Since the conditional measure $P_{\widehat{Y}|X}(\cdot|x)$, $x \in \mathbb{R}$ is continuous in x , and $\lim_{x \rightarrow \infty} P_{\widehat{Y}|X}(\mathcal{A}|x) = \mathbb{1}(\hat{y} \in \mathcal{A})$, $\mathcal{A} \in \mathbb{B}$ for some fixed \hat{y} , the conditions in the proof of [43, Prop. 1] hold, and the optimal input distribution has bounded support. Then, using the extension of Witsenhausen's result [44] given in [43, Prop. 2], the optimal input distribution is discrete and takes at most $2n_q + 1$ values. This completes the proof of converse. To prove achievability, it suffices to show that one can choose the set of functions $f_{a_j,j}(\cdot)$, $j \in [n_q]$ and quantization thresholds t_j , $j \in [n_q]$ such that the resulting quantizer operates as described in the theorem statement, i.e., it generates $\widehat{Y} = Q(hX + N)$ where $Q(y) = k$ if $y \in [t_k, t_{k+1}]$, $k \in \{1, \dots, 2n_q\}$ and $Q(y) = 0$ if $y > t_{2n_q}$ or $y < t_1$. To this end, let \mathbf{t}^* be the optimal quantizer thresholds in (2). Let $r_1, r_2, \dots, r_{2n_q}$ be the elements of \mathbf{t}^* written in non-decreasing order. Define a quantizer with associated analog functions $f_{a,j}(y) \triangleq |y - \frac{r_j + r_{n_q+j}}{2}|$ and $t_j = \frac{r_{n_q+j} - r_j}{2}$. Note that $t_j > 0$ since r_j , $j \in [n_q]$ are non-decreasing. Then, similar to the proof of Proposition 1, the quantization rule gives distinct outputs for $y \in [r_k, r_{k+1}]$, $k \in \{1, \dots, 2n_q\}$ and $y \in [r_{2n_q}, \infty) \cup [-\infty, r_1]$ as desired. \square

Remark 1. *The capacity expression in Equation (2) can be evaluated numerically, e.g. via the cutting plane algorithm [43], [45], or extension of Blahut-Arimoto algorithm in [46].*

3) *Low-resolution ADCs and Concatenated Sequences of Envelop Detectors:* Next, we consider systems with $\delta > 1$, $\ell > 2$. Recall that for $\delta > 1$, each $f_j(y)$, $j \in [n_q]$ is of the form $f_j(y) = A_\delta(y, a_j^\delta) = |A_{\delta-1}(y, a_j^{\delta-1}) - a_{j,\delta}|$, where $A_1(y, a_{j,1}) = |y - a_{j,1}|$. For tractability, we use the notation $f_{a_j^\delta,j}(y) \triangleq A_\delta(y, a_j^\delta)$ to explicitly denote the bias vector a_j^δ used for the j th analog function. The following example introduces the concept of degenerate bias vectors for a given threshold matrix \mathbf{t} .

Example 2. *Let $n_q = 1$, $\ell = 3$, $\delta = 2$, and consider the thresholds $t_{1,1} = 1$ and $t_{1,2} = 2$. Given a bias vector, (a_1, a_2) , the associated analog function is $f_{a_1^\delta,1}(y) = ||y - a_1| - a_2|$. The ADC output is*

$$Q(y) = \begin{cases} 0 & \text{if } ||y - a_1| - a_2| < 1 \\ 1 & \text{if } 1 < ||y - a_1| - a_2| < 2 \\ 2 & \text{if } 2 < ||y - a_1| - a_2| \end{cases}$$

Note that if $a_2 - 1 < 0$, then this would be equivalent with:

$$Q(y) = \begin{cases} 0 & \text{if } |y - a_1| < 1 + a_2 \\ 1 & \text{if } 1 < |y - a_1| < 2 + a_2 \\ 2 & \text{if } 2 + a_2 < |y - a_1| \end{cases}$$

In this case, the second envelope detector does not affect the quantization process and can be omitted without change in quantizer output, i.e., the input to the corresponding absolute value is always positive, so it can be removed.

We call bias vectors $a_j^\delta, j \in [n_q]$ which yield redundant envelope detectors, such as the one in Example 2, degenerate bias vectors. The following proposition characterizes necessary and sufficient conditions for non-degeneracy of bias vectors.

Proposition 2 (Non-Degenerate Bias Vectors). *Let the threshold vector corresponding to the j th ADC be $t^{\ell-1}$, where $j \in [n_q]$. The bias vector of the corresponding analog operator $f_j(\cdot)$ is non-degenerate if and only if:*

$$0 < t_1 + \sum_{i=2}^{\delta} (-1)^{b_i} a_i, \quad \forall b_i \in \{-1, 1\}. \quad (3)$$

The proof follows by noting that from definition $0 < t_1 < t_2 < \dots < t_\ell - 1$ so that Equation (3) is sufficient to ensure non-degeneracy. We will use the following notion of a fully-symmetric vector in deriving properties of roots of quantizers with non-degenerative bias vectors.

Definition 2 (Fully-Symmetric Vector). *A vector $\mathbf{b} = (b_1, b_2, \dots, b_{2^n})$ is called symmetric if $b_i + b_{2^n-i} = b_j + b_{2^n-j}, i, j \in [2^n - 1]$. \mathbf{b} is called fully-symmetric if it is symmetric and the vectors $(b_1, b_2, \dots, b_{2^{n-1}})$ and $(b_{2^{n-1}+1}, b_{2^{n-1}+2}, \dots, b_{2^n})$ are both fully-symmetric for $n > 2$ and symmetric for $n = 2$.*

For instance, the vector $\mathbf{b} = (-7, -6, -5 - 4, 4, 5, 6, 7)$ is fully symmetric since it is symmetric and $(-7, -6, -5 - 4)$ and $(4, 5, 6, 7)$ are both symmetric.

Proposition 3 (Properties of Roots of Associated Analog Functions). *Consider a quantizer $Q(\cdot)$ with threshold matrix $\mathbf{t} \in \mathbb{R}^{n_q \times (\ell-1)}$, and analog processing functions $f_j(\cdot), j \in n_q$, such that the corresponding bias vectors are non-degenerate and $f_{j,k}(\cdot) \triangleq f_j(\cdot) - t(j, k), j \in [n_q], k \in [\ell - 1]$ do not have repeated roots. Let $r_1, r_2, \dots, r_\gamma$ be the increasing sequence of roots, where $\gamma \triangleq (\ell - 1)n_q 2^\delta$. Then, there exists a partition $\{\mathcal{P}_{j,k}, j \in [n_q], k \in [\ell - 1]\}$ of $[\gamma]$ such that*

- 1) $|\mathcal{P}_{j,k}| = 2^\delta, j \in [n_q], k \in [\ell - 1]$.
- 2) For $j \in [n_q], k \in [\ell - 1]$, let $\mathcal{P}_{j,k} = \{i_1, i_2, \dots, i_{2^\delta}\}$, where $i_j < i_{j'}$ for $j < j'$. The vector $(r_{i_1}, r_{i_2}, \dots, r_{i_{2^\delta}})$ is fully-symmetric,
- 3) For all $j \in [n_q], k, k' \in [\ell - 1]$, we have $r_{i_t} - r'_{i'_t} = r_{i'_t} - r'_{i_t}, i_t, i'_t \in [2^\delta]$, where $r_{i_t}, r_{i'_t} \in \mathcal{P}_{j,k}$ and $r'_{i_t}, r'_{i'_t} \in \mathcal{P}_{j,k'}$.

The proof follows by taking each $\mathcal{P}_{j,k}$ to be the ordered set of roots of $f_{j,k}$ for a given $j \in [n_q], k \in [\ell - 1]$ and using properties of the absolute value. The following proposition states several useful properties for

the code associated of a quantizer $Q(\cdot)$.

Proposition 4 (Properties of the Associated Code). *Consider a quantizer $Q(\cdot)$ with threshold matrix $\mathbf{t} \in \mathbb{R}^{n_q \times (\ell-1)}$ such that $0 < t(i, j) < t(i, j'), i \in [n_q], j, j' \in [\ell-1], j < j'$, and analog processing functions $f_j(\cdot), j \in [n_q]$, such that the corresponding bias vectors are non-degenerate and $f_{j,k}(\cdot) \triangleq f_j(\cdot) - t(j, k), j \in [n_q], k \in [\ell-1]$ do not have repeated roots. The associated code C satisfies the following:*

- 1) *The number of codewords in C is equal to $\gamma \triangleq (\ell-1)n_q2^\delta + 1$, i.e. $C = (\mathbf{c}_0, \mathbf{c}_1, \dots, \mathbf{c}_{\gamma-1})$.*
- 2) *All elements of the first codeword \mathbf{c}_0 are equal to $\ell-1$, i.e. $c_{i,0} = \ell-1, i \in \{0, 1, \dots, \gamma-1\}$.*
- 3) *Consecutive codewords differ in only one position, and their L_1 distance is equal to one, i.e. $\sum_{j=1}^{n_q} |c_{i,j} - c_{i+1,j}| = 1, i \in \{0, 1, \dots, \gamma-1\}$.*
- 4) *The transition count at every position is $\kappa_j = \frac{\gamma}{n_q} = (\ell-1)2^\delta, j \in [n_q]$.*
- 5) *Let i_1, i_2, \dots, i_k be the non-decreasingly ordered indices of codewords, where the j th element has value-transitions. Then, the sequence $(c_{i_1,j}, c_{i_2,j}, \dots, c_{i_k,j})$ is periodic, in each period it takes all values between 0 and $\ell-1$, and $|c_{i_k,j} - c_{i_{k+1},j}| = 1, k \in [k-1]$ holds. Furthermore, $c_{i_1,j} \in \{0, \ell-1\}$.*
- 6) $|C| \leq \min(\ell^{n_q}, (\ell-1)n_q2^\delta)$.

Proposition 4 is an extension of the properties shown in the proof of Theorem 1. We provide a brief justification of each property in the following. Property 1 follows by the fact that the number of codewords in C is equal to the number of roots of $f_{j,k}, j \in [n_q], k \in [\ell-1]$ plus one (e.g., see Figure 3). Property 2 and 6 follow by a similar argument as Equation (1) in proof of Proposition 1. Properties 3 and 5 follow by the fact that each root of $f_{j,k}, j \in [n_q], k \in [\ell-1]$ corresponds to a value transition in the output of exactly one of the ADCs (since the roots are not repeated) and at each transition the value changes either one unit up or down since in the input crosses one threshold at a time at its value is changed continuously. Property 4 follows by the fact that the transition count at each position is equal to the number of roots of $f_{j,k}, k \in [\ell-1]$ for a fixed $j \in [n_q]$.

As a step towards characterizing capacity when $\ell > 2, \delta > 1$, we first study the capacity region for systems with one-bit ADCs, i.e., $\ell = 2, \delta > 1$. To this end, we prove two useful propositions. The first one shows that given an ordered set C satisfying the properties in Proposition 4 and a sequence of real numbers $(r_1, r_2, \dots, r_\gamma)$ satisfying the properties in Proposition 3, one can always construct a quantizer whose associated code is equal to C and whose polynomial roots sequence is $(r_1, r_2, \dots, r_\gamma)$. The second proposition provides conditions under which there exists a code satisfying the properties in Proposition 4. The proof ideas follow techniques used in study of balanced and locally balanced gray codes [47], [48]. Combining the two results allows us to characterize the necessary and sufficient conditions for existence of quantizers with desirable properties.

In the statement of the following proposition, for a given code C , we have used the notation $\xi_1, \xi_2, \dots, \xi_{\gamma-1}$ for the transition sequence of C . That is, $\xi_k, k \in \{1, \dots, \gamma-1\}$ is the bit position which is different between \mathbf{c}_{k-1} and \mathbf{c}_k . We have defined the transition sets $\mathcal{I}_j \triangleq \{s | \xi_s = j\}, j \in [n_q]$. Note from Property 5) in Proposition 4, we have $|\mathcal{I}_j| = \kappa_j = 2^\delta$.

Proposition 5 (Quantizer Construction). *Let $\ell = 2, n_q \in \mathbb{N}$ and $\delta > 1$ and consider an ordered set $C \subset \{0, 1\}^{n_q}$ satisfying properties 1)-5) in Proposition 4, and a sequence of increasing real numbers $r_1, r_2, \dots, r_\gamma$, where $\gamma = n_q 2^\delta$, such that $(r_{i_s}, s \in \mathcal{I}_j)$ is fully-symmetric for all $j \in [n_q]$, where \mathcal{I}_j are the transition sets of C . Then, there exists a quantizer $Q(\cdot)$ with associated analog functions $f_j(\cdot), j \in [n_q]$ such that its associated code is C , and $r_1, r_2, \dots, r_\gamma$ is the non-decreasing sequence of roots of its associated analog functions $f_{j,k}(\cdot), j \in [n_q], k \in [\ell - 1]$.*

Proof. For $j \in [n_q]$ and non-decreasing vector $(r_{i_1}, r_{i_2}, \dots, r_{i_{2^\delta}})$ where $i_\lambda \in \mathcal{I}_j, j \in [n_q], \lambda \in [2^\delta]$, define

$$a_{1,j} \triangleq \frac{r_{i_1} + r_{i_{2^\delta}}}{2}, \quad a_{s,j} \triangleq \frac{r_{i_{2^\delta}} + r_{i_{\eta_s}}}{2} - \sum_{s'=1}^{s-1} a_{s',j}, \quad 1 < s \leq \delta,$$

$$t_j \triangleq r_{i_{2^\delta}} - \sum_{s'=1}^{\delta-1} a_{s',j}, \quad 1 < s \leq \delta$$

where $\eta_s \triangleq 2^\delta - \sum_{s'=1}^{s-1} 2^{\delta-s'} + 1, s > 1$. Consider a quantizer $Q(\cdot)$ with ADC thresholds $t(1 : n_q)$ and associated analog functions $f_j(y) \triangleq A_\delta(x, a^\delta), j \in [n_q]$. Then, $r_1, r_2, \dots, r_\gamma$ are the non-decreasing sequence of roots of $f_j(\cdot), j \in [n_q]$, and the associated code of the quantizer $Q(\cdot)$ is C as desired. \square

Proposition 6. (Code Construction) *Let $\ell = 2, n_q \in \mathbb{N}$, and $\kappa_1, \kappa_2, \dots, \kappa_{n_q}$ be even numbers such that $|\kappa_j - \kappa_{j'}| \leq 2, j, j' \in [n_q]$. Then, there exists a code C with transition count at position j equal to $\kappa_j, j \in [n_q]$ satisfying properties 1), 2), 3), and 5) in Proposition 4 such that $|C| = \min\{2^{n_q}, \sum_{j=1}^{n_q} \kappa_j\}$. Particularly, if $\kappa_j = 2^\delta, j \in [n_q]$, then there exists C with $|C| = \min\{2^{n_q}, n_q 2^\delta\}$ satisfying properties 1)-5) in Proposition 4.*

Proof. Please refer to Appendix A. \square

Using Propositions 5 and 6, we characterize the channel capacity for $\ell = 2$ and $\delta > 1$. Let us define $\Gamma_2 \triangleq \min(2^{n_q}, n_q 2^\delta + 1)$ and the set $\mathcal{T}_{\Gamma_2} \subseteq \mathbb{R}^{\Gamma_2-1}$ as the set of sequences of increasing real numbers $r_1, r_2, \dots, r_\gamma$, where $\gamma = n_q 2^\delta$ for which there exists a partition $\{\mathcal{I}_j, j \in [n_q]\}$ of $[\delta]$ such that $(r_{i_s}, s \in \mathcal{I}_j)$ is fully-symmetric for all $j \in [n_q]$, and there exists a code satisfying Properties 1)-5) in Proposition 4 whose transition sets are equal to $\mathcal{I}_j, j \in [n_q]$ and which has exactly one repeated codeword, i.e., only the first and last codewords are repeated. The following theorem characterizes the channel capacity.

Theorem 2. Consider a system parametrized by $(P, h, n_q, \delta, \ell)$, where $P > 0, h \in \mathbb{R}, n_q \in \mathbb{N}, \delta > 1$, and $\ell = 2$. Then, the capacity is given by:

$$C_{\text{env}}(P, h, n_q, \delta, \ell) = \sup_{\mathbf{x} \in \mathbb{R}^{\Gamma_2}} \sup_{P_{\mathbf{x}} \in \mathcal{P}_{\mathbf{x}}(P)} \sup_{\mathbf{t} \in \mathcal{T}_{\Gamma_2}} I(X; \widehat{Y}), \quad (4)$$

where $\widehat{Y} = Q(hX + N)$, $N \sim \mathcal{N}(0, 1)$, $\mathcal{P}_{\mathbf{x}}(P)$ is the set of distributions on $\{x_1, x_2, \dots, x_{\Gamma_2}\}$ such that $\mathbb{E}(X^2) \leq P$, and $Q(y) = k$ if $y \in [t_k, t_{k+1}]$, $k \in \{1, \dots, \Gamma_2 - 1\}$ and $Q(y) = 0$ if $y > t_{\Gamma_2-1}$ or $y < t_1$.

The proof follows by similar arguments as in the proof of Theorem 1. The converse follows from Proposition 4 Item 4). Achievability follows from Proposition 6.

The region given in Theorem 2 is difficult to analyze since finding the set \mathcal{T}_{Γ_2} may be computationally complex. Inner bounds to the achievable region may be numerically derived by assuming additional symmetry restriction such as uniform quantization restrictions. This is studied in more detail in the numerical evaluations provided in Section V.

For scenarios with $\ell > 2, \delta > 1$, let us define $\Gamma_\ell \triangleq \min(2^{n_q}, (\ell - 1)n_q 2^\delta + 1)$ and the set $\mathcal{T}_{\Gamma_\ell} \subseteq \mathbb{R}^{\Gamma_\ell-1}$ as the set of sequences of increasing real numbers $r_1, r_2, \dots, r_{\Gamma_\ell}$ satisfying the properties in Proposition 3, for which there exists a code C satisfying Properties 1)-5) in Proposition 4 such that i) the sets $\mathcal{P}_{j,k}, j \in [n_q], k \in [\ell - 1]$ in 3 are the indices of the codewords of C which have transition to or from value k in their j th element, and ii) C has exactly one repeated codeword, i.e., only the first and last codewords are repeated. The following theorem characterizes the channel capacity. The proof follows from Propositions 4 and 6 similar to the arguments given in the proof of Theorem 1.

Theorem 3. Consider a system parametrized by $(P, h, n_q, \delta, \ell)$, where $P > 0, h \in \mathbb{R}, n_q \in \mathbb{N}$, and $\ell, \delta \in \mathbb{N}$. Let Γ_ℓ be the maximum size of codes satisfying condition 1)-5) in Proposition 4. Then,

$$C_{\text{env}}(P, h, n_q, \delta, \ell) = \sup_{\mathbf{x} \in \mathbb{R}^{\Gamma_\ell}} \sup_{P_{\mathbf{x}} \in \mathcal{P}_{\mathbf{x}}} \sup_{\mathbf{t} \in \mathcal{T}_{\Gamma_\ell}} I(X; \widehat{Y}), \quad (5)$$

where Γ_ℓ is the maximum number of unique codewords in a code C satisfying Properties 1)-5) in Proposition 4, and $\widehat{Y} = Q(hX + N)$, $N \sim \mathcal{N}(0, 1)$, $\mathcal{P}_{\mathbf{x}}(P)$ consists of distributions on $\{x_1, x_2, \dots, x_{\Gamma_\ell}\}$ such that $\mathbb{E}(X^2) \leq P$, and $Q(y) = k$ if $y \in [t_k, t_{k+1}]$, $k \in [\Gamma_\ell - 1]$ and $Q(y) = 0$ if $y > t_{\Gamma_\ell-1}$ or $y < t_1$.

Optimizing (5) requires calculating Γ_ℓ . The total number of codes satisfying conditions 1)-5) in Proposition 4 is bounded from above by $\binom{(\ell-1)2^\delta n_q}{(\ell-1)2^\delta, (\ell-1)2^\delta, \dots, (\ell-1)2^\delta}$. Hence, for systems with a few low resolution ADCs and small δ ($\delta = 1, 2$), one can find Γ_ℓ by searching over all such codes.

III. ANALOG BEAMFORMING ARCHITECTURE WITH POLYNOMIAL OPERATORS

In the previous section, we investigated the channel capacity under analog beamforming when sequences of concatenated envelop detectors are used for analog signal processing. In this section, we evaluate the

resulting channel capacity when analog polynomial operators are used instead of envelop detectors. We define the set of implementable analog operators

$$\mathcal{F}_{poly}^\delta \triangleq \{f(x) = \sum_{i=0}^{\delta} a_i x^i, x \in \mathbb{R} | a_i \in \mathbb{R}, i = 0, 1, \dots, \delta\}.$$

We denote the resulting channel capacity by $C_{poly}(P, h, n_q, \delta, \ell)$.

Example 3 (Associated Code). Let $n_q = \delta = 2$ and $\ell = 3$ and consider a quantizer characterized by polynomials $f_{a,1}(y) = y^2 + 2y$ and $f_{a,2}(y) = y^2 + 3y, y \in \mathbb{R}$, and thresholds

$$t(1, 1) = 3, \quad t(1, 2) = 0, \quad t(2, 1) = 10, \quad t(2, 2) = 18,$$

We have:

$$\begin{aligned} f_{a,1,1}(y) &= y^2 + 2y - 3, & f_{a,1,2}(y) &= y^2 + 2y \\ f_{a,2,1}(y) &= y^2 + 3y - 10, & f_{a,2,2}(y) &= y^2 + 3y - 18. \end{aligned}$$

The ordered root sequence is $(r_1, r_2, \dots, r_8) = (-6, -5, -3, -2, 0, 1, 2, 3)$. The associated partition is:

$$\begin{aligned} \mathbf{P} = \{ & [-\infty, -6), (-6, -5), (-5, -3), (-3, -2), (-2, 0), \\ & (0, 1), (1, 2), (2, 3), (3, \infty) \}. \end{aligned}$$

The associated code is given by 22, 21, 20, 10, 00, 10, 20, 21, 22. The size of the code is $|C| = 5$. The high SNR capacity of a channel using this quantizer at the receiver is $\log |\mathbf{P}| = \log |C| = \log 5$.

As a first step, we show the following proposition about properties of codes and their associated polynomial functions which is analogous to Proposition 4 which addressed codes and their associated envelop-detector-based analog processing functions. The proof follows by similar arguments as that of Proposition 4 and is omitted for brevity.

Proposition 7. Consider a quantizer $Q(\cdot)$ with threshold matrix $\mathbf{t} \in \mathbb{R}^{n_q \times (\ell-1)}$ and associated polynomials $f_j(\cdot) \in \mathcal{F}_{poly}^\delta, j \in [n_q]$, such that $f_{j,k}(\cdot) \triangleq f_j(\cdot) - t(j, k), j \in [n_q], k \in [\ell-1]$ do not have repeated roots. The associated code C satisfies the following:

- 1) The number of codewords in C is equal to $\gamma \triangleq (\ell-1)\delta n_q + 1$, i.e. $C = (\mathbf{c}_0, \mathbf{c}_1, \dots, \mathbf{c}_{\gamma-1})$.
- 2) All elements of the first codeword \mathbf{c}_0 are either equal to $\ell-1$ or equal to 0, i.e. $c_{i,0} = 0, i \in \{0, 1, \dots, \gamma-1\}$ or $c_{i,0} = \ell-1, i \in \{0, 1, \dots, \gamma-1\}$.
- 3) Consecutive codewords differ in only one position, and their L_1 distance is equal to one, i.e. $\sum_{j=1}^{n_q} |c_{i,j} - c_{i+1,j}| = 1, i \in \{0, 1, \dots, \gamma-1\}$.
- 4) The transition count at every position is $\kappa_j = \frac{\gamma}{n_q} = (\ell-1)\delta, j \in [n_q]$.

- 5) Let i_1, i_2, \dots, i_k be the non-decreasingly ordered indices of codewords where the j th element has value-transitions. Then, the sequence $(c_{i_1,j}, c_{i_2,j}, \dots, c_{i_k,j})$ is periodic, in each period it takes all values between 0 and $\ell - 1$, and $|c_{i_k,j} - c_{i_{k+1},j}| = 1, k \in [k - 1]$ holds. Furthermore, $c_{i_1,j} \in \{0, \ell - 1\}$.
- 6) If δ is even, then $|C| \leq \min(\ell^{n_q}, (\ell - 1)\delta n_q)$ and if δ is odd, then $|C| \leq \min(\ell^{n_q}, (\ell - 1)\delta n_q + 1)$

Using Proposition 6 and Proposition 7, and following the arguments in the proof of Theorem 2, one can prove the following theorem.

Theorem 4. Consider a system parametrized by $(P, h, n_q, \delta, \ell)$, where $P > 0, h \in \mathbb{R}, n_q \in \mathbb{N}$, and $\ell = 2$. Then,

$$C_{poly}(P, h, n_q, \delta, \ell) = \sup_{\mathbf{x} \in \mathbb{R}^\Gamma} \sup_{P_X \in \mathcal{P}_X(P)} \sup_{\mathbf{t} \in \mathbb{R}^{\Gamma-1}} I(X; \widehat{Y}), \quad (6)$$

if δ is even and

$$\begin{aligned} \sup_{\mathbf{x} \in \mathbb{R}^\Gamma} \sup_{P_X \in \mathcal{P}_X(P)} \sup_{\mathbf{t} \in \mathbb{R}^{\Gamma-1}} I(X; \widehat{Y}) &\leq C_Q(P, h, n_q, \delta, \ell) \\ &\leq \sup_{\mathbf{x} \in \mathbb{R}^{\Gamma'}} \sup_{P_X \in \mathcal{P}_X(P)} \sup_{\mathbf{t} \in \mathbb{R}^{\Gamma'-1}} I(X; \widehat{Y}), \end{aligned} \quad (7)$$

if δ is odd, where $\Gamma \triangleq \min(2^{n_q}, \delta n_q)$, $\Gamma' \triangleq \min(2^{n_q}, \delta n_q + 1)$, $\widehat{Y} = Q(hX + N)$, $N \sim \mathcal{N}(0, 1)$, $\mathcal{P}_X(P)$ is the set of distributions on $\{x_1, x_2, \dots, x_\Gamma\}$ such that $\mathbb{E}(X^2) \leq P$, and $Q(y) = k$ if $y \in [t_k, t_{k+1}]$, $k \in \{1, \dots, \Gamma - 1\}$ and $Q(y) = 0$ if $y > t_{\Gamma-1}$ or $y < t_1$.

We make the following observations regarding the achievable regions in Theorems 3 and 4:

- 1) It can be noted from Equations (4) and (7) that the capacity expression for odd and even values of δ are not the same. This is due to Property 6) in Proposition 7 which gives different number of unique codewords for odd and even δ . The reason is that while even degree polynomials yield the same output sign as their input converges to $-\infty$ and ∞ , for odd degree polynomials the output signs are different as their input converges to $-\infty$ and ∞ . This can potentially yield a larger number of unique codewords in the associated code of the quantizer since the first and last codeword are not equal to each other. This is in contrast with Theorem 3, where the capacity expression is the same for even and odd values of δ . The reason is that for absolute values the output sign is positive as their input converges to $-\infty$ and ∞ .
- 2) The region given in Theorem 4 strictly contains that of Theorem 3 for the same value of Γ . The reason is that envelope detectors generate absolute value functions which force a symmetric structure on the Voronoi regions of $Q(\cdot)$. This manifests in the fully-symmetric condition $\mathbf{t} \in \mathcal{T}_\Gamma$ in Theorem 3 and the properties given in Proposition 3; whereas for polynomial functions, no such symmetry is required and

hence the optimization in Theorem 4 is over all $\mathbf{t} \in \mathbb{R}^\Gamma$. However, as shown in Section VI generating polynomial operators of degree up to δ requires a larger power budget compared to concatenating δ envelop detectors. This points to a rate-power tradeoff in using envelop detectors and polynomials operators.

3) One potential approach to improve upon the capacity of the system in Theorem 3 is to augment the envelop detectors by linearly combining their output with the original signal. That is, to generate operators of the form $f(y) = |y - a| + by, a, b \in \mathbb{R}$ instead of $f(y) = |y - a|, a \in \mathbb{R}$. This removes the fully-symmetric condition $\mathbf{t} \in \mathcal{T}_\Gamma$ in Theorem 3 and yields a larger channel capacity. However, such linear combinations are challenging to implement using analog circuits due to timing issues in synchronizing the output of the envelop detector with the original signal. We hope to address these implementation challenges in future works.

4) For envelop detectors, the dimension Γ is equal to $n_q(\ell - 1)2^\delta$, whereas for polynomial operators, it is equal to $n_q(\ell - 1)\delta$. So, the dimension of the optimization space increases faster when concatenating envelop detectors compared to when increasing the polynomial degree. That is, at high SNRs, the capacity in Theorem 3 is larger than that of Theorem 4 for the same value of $\delta > 1$. This is also observed in the numerical evaluations in Section V.

IV. A HYBRID BEAMFORMING ARCHITECTURE WITH ONE-BIT ADCs

In the previous sections, we have investigated the channel capacity under analog beamforming equipped with different collections of implementable analog functions. In this section, we consider hybrid beamforming with one-bit ADCs, where the beamforming vector at the receiver $\mathbf{w} \in \mathbb{R}^{n_r \times n_s}$ maps the received signal Y^{n_r} to \tilde{Y}^{n_s} , where $n_s > 1$ (Figure 1). In this case, we provide a quantization setup, using envelop detectors, which accommodates QAM modulation, and provide inner bounds to the system capacity. In the next section, we numerically evaluate the resulting capacity and provide comparisons with prior works.

A. Quantizer Construction

We assume that $n_q > n_s$, otherwise, one can use analog beamformers to further reduce the dimension of the beamformer output without performance loss in terms of achievable rates. As mentioned in Section II-A a quantizer is characterized by its analog processing functions $f_j(\cdot), j \in [n_q]$ and one-bit ADC thresholds $t^{n_q} \in \mathbb{R}^{n_q}$. Let us fix a threshold step parameter $\zeta > 0$. We take the analog processing functions as follows:

$$f_j(\tilde{\mathbf{y}}^{n_s}) = \begin{cases} \tilde{y}_j & \text{if } j \leq n_s, \\ \lfloor \tilde{y}_j \rfloor & \text{if } j > n_s, \end{cases}$$

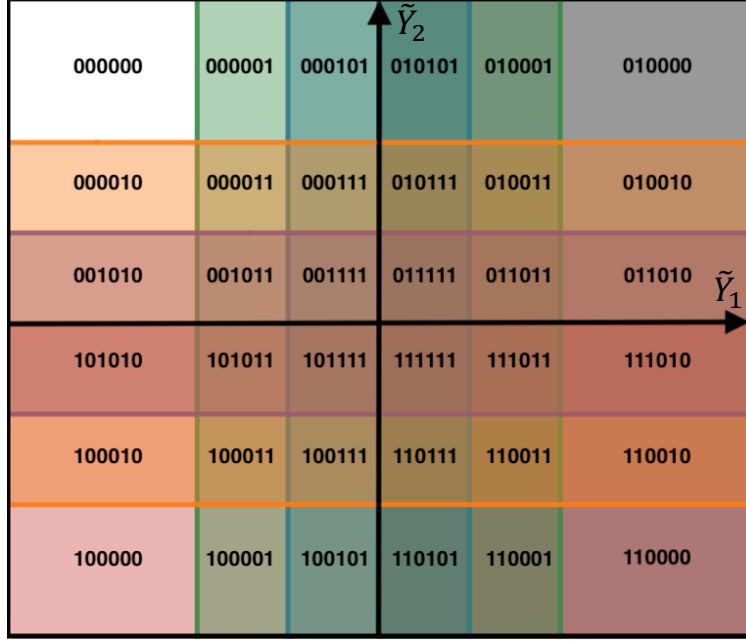


Fig. 4: The quantizer outputs and Voronoi regions in Example 4.

where \bar{j} is the module n_s residual of j . We take the threshold values as follows:

$$t_j = \begin{cases} 0 & \text{if } j \leq n_s, \\ \lfloor \frac{j}{n_q} \rfloor \zeta & \text{if } j > n_s. \end{cases}$$

This choice is clarified through the following example.

Example 4. Let $n_s = 2$, $n_q = 6$, and $\zeta = 1$. Then, for the construction described above, the six one-bit ADC operations are as follows:

$$Q_1 : \bar{y}_1 \leq 0, \quad Q_2 : \bar{y}_2 \leq 0, \quad Q_3 : |\bar{y}_1| \leq 1,$$

$$Q_4 : |\bar{y}_2| \leq 1, \quad Q_5 : |\bar{y}_1| \leq 2, \quad Q_6 : |\bar{y}_2| \leq 2.$$

The quantizer outputs are shown in Figure 4. Note that this resembles a 16-QAM modulation.

B. Achievable Rates at High SNR

As argued in Section II, the high SNR capacity is equal to the maximum number of quantization regions which can be generated given the number of one-bit ADCs n_q and set of implementable analog functions \mathcal{F} . The following theorem provides upper and lower bounds on the high SNR channel capacity of beamforming architectures equipped with envelope detectors for analog signal processing.

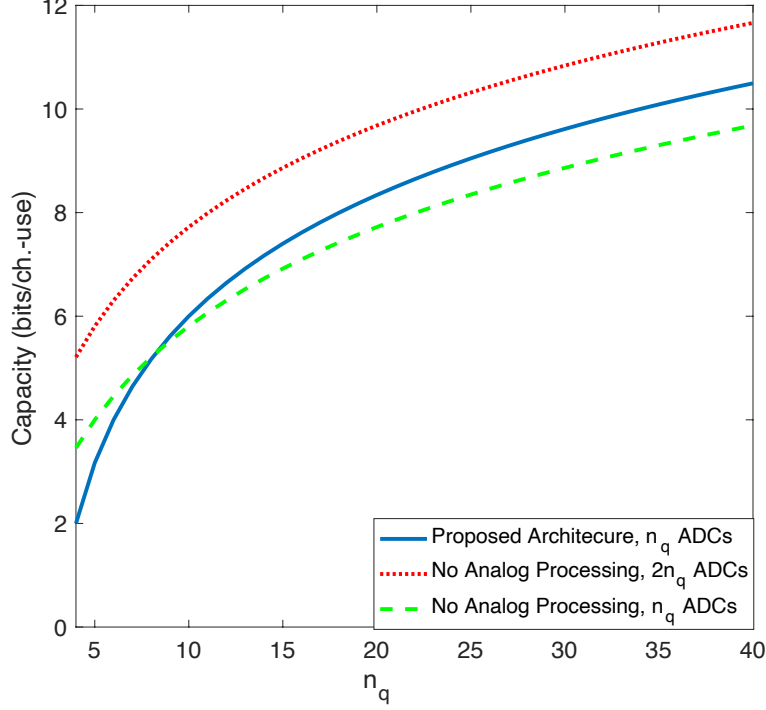


Fig. 5: Channel capacity for i) the proposed architecture and n_q one-bit ADCs (lower-bound in Theorem 5), ii) no analog processing prior to quantization and $2n_q$ one-bit ADCs (upper-bound in Theorem 5) and iii) no analog processing prior to quantization and n_q one-bit ADCs ([41]).

Theorem 5. Assume that the channel matrix observed after beamforming is full-rank, i.e. the rank of $\mathbf{w}^H \mathbf{h} \mathbf{f}$ is equal to n_s . Let $C_{env}(P, n_s, n_q, \ell, \delta)$ denote the channel capacity under power constrain P . Then,

$$n_s \left(1 + \log \left(\frac{n_q - n_s}{n_s} \right) \right) \leq \lim_{P \rightarrow \infty} C_{env}(P, n_s, n_q, 2, 1) \leq \log \sum_{k=0}^{n_s} \binom{2n_q}{k}. \quad (8)$$

The lower bound in Equation (8) is achieved by the quantizer described in this section. To see this, note that by construction, the quantizer partitions each axis into $2 \left(\frac{n_q - n_s}{n_s} \right)$ intervals, and each resulting quantization region is mapped to a unique quantizer output (e.g., Figure 4). So, the total number of unique quantizer outputs is $|C| = 2^{n_s \left(\frac{n_q - n_s}{n_s} \right) n_s}$. The result follows by noting that the communication rate is $\log |C|$. The upper bound follows by counting the number of partition regions generated by $2n_q$ hyperplanes in general position in the n_s -dimensional Euclidean space (e.g. [41], [49]). Figure 5 provides numerical simulations of the i) upper bounds and ii) lower bounds in Equation (8) and iii) the high SNR channel capacity under hybrid beamforming without analog processing derived in [41] for $n_s = 3$. It can be observed that the proposed architecture outperforms the one in [41] if the number of one-bit ADCs is larger than $n_q = 8$.

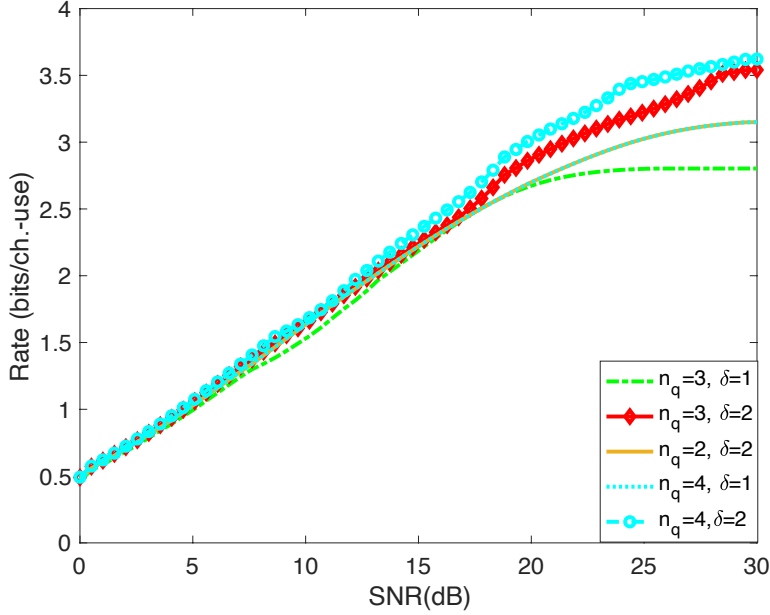


Fig. 6: The set of achievable rates for various values of (n_q, ℓ, δ) for architectures using envelop detectors.

V. NUMERICAL ANALYSIS OF CHANNEL CAPACITY

In this section, we provide a numerical analysis of the capacity bounds derived in the prequel and evaluate the gains due to the use of nonlinear analog components in the receiver terminal.

A. Capacity Evaluation for Envelop Detector Architectures

We compute an inner-bound to the capacity expression in Theorem 3. To this end, we first use the extension of the Blahut-Arimoto algorithm to discrete memoryless channels with input cost constraints given in [46] to find the best input distribution. Then, we conduct a brute-force search over all possible uniform quantizers. In order to find the mass points of X , we discretize the real-line using a grid with step-size 0.1, and optimize the distribution over the resulting discrete space. Fig. 6 shows the resulting achievable rates for SNRs in the range of 0 to 30 dB for various values of (n_q, ℓ, δ) . Observe that without nonlinear analog processing, for $\ell = 2$, the high SNR capacity is $\log n_q + 1$ [41]. So, for instance, for $n_q = \delta = 2$, the inner bound in Figure 6 surpasses the high SNR capacity without nonlinear analog processing for SNRs higher than 15dB, and its high SNR capacity is more than 60% greater than the case when there is no nonlinear analog processing.

B. Capacity Evaluation for Polynomial Operator Architectures

We numerically evaluate the inner bound to the capacity region given in Theorem 4. Similar to the previous case, we first use the extension of the Blahut-Arimoto algorithm to find the best input distribution.

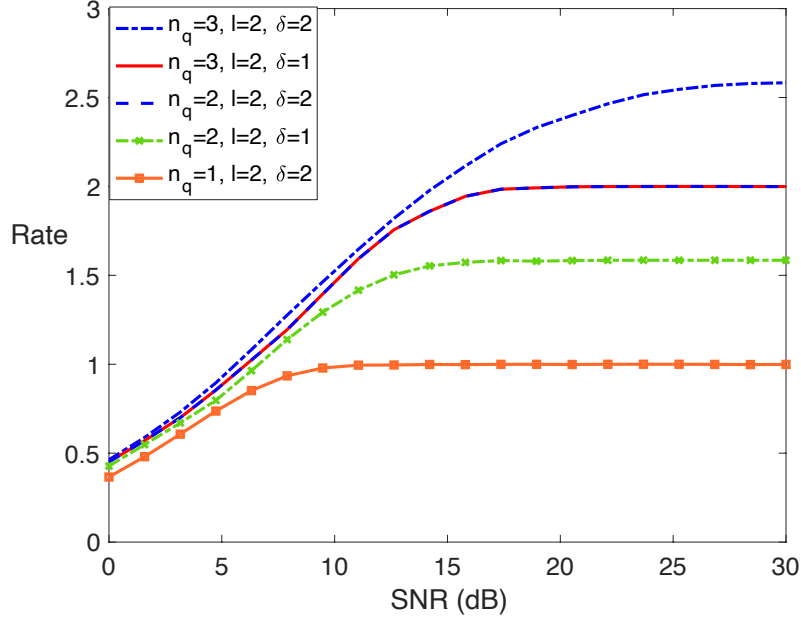


Fig. 7: The set of achievable rates for various values of (n_q, ℓ, δ) for architectures using polynomial operators.

Then, we conduct a brute-force search over all possible symmetric threshold vectors, where a vector \mathbf{t} is symmetric if $\mathbf{t} = -\mathbf{t}$ [43]. To find the mass points of X , we discretize the real-line using a grid with step-size 0.1, and optimize the distribution over the resulting discrete space. Figure 7 shows the resulting achievable rates for SNRs in the range of 0 to 30 dB for various values of (n_q, ℓ, δ) . It can be observed that the performance improvements due to the use of higher degree polynomials are more significant at high SNRs. Furthermore, it can be observed that the set of achievable rates only depends on $\min(\ell^{n_q}, (\ell - 1)\delta n_q + 1)$. As a result, for instance the achievable rate when $n_q = 2, \ell = 2, \delta = 2$ is the same as that of $n_q = 3, \ell = 2, \delta = 1$ as shown in the figure. So, in this case, using higher degree polynomials can compensate for a lower number of ADCs. On the other hand, the achievable rate for $n_q = 3, \ell = 2, \delta = 1$ is lower than that of $n_q = 3, \ell = 2, \delta = 2$ as shown in the figure. So, using higher degree polynomials leads to rate improvements in this scenario.

C. Achievable Inner-Bound for Hybrid Beamforming with Envelop Detectors

We numerically evaluate the inner-bound to the channel capacity which is achievable using the beamforming architecture described in Section IV. We have simulated the communication system for $n_s = 2$, $\ell = 2$, and $n_q \in \{5, 6\}$ and found an estimate of the achievable rates empirically. The results are shown in Figure 9. To perform the simulation, we have optimized the threshold parameter ζ , the input alphabet values $\mathbf{x} \in \mathbb{R}^2$, and the probability distribution P_X on the alphabet of the input points using a

gradient descent optimization method. We have simulated the channel by generating 15000 independent and identically distributed samples of noise vectors and input messages. We have used the empirical observations to estimate transition probability of the discrete channel resulting from the quantization process. We have used the Blahut-Arimoto algorithm to find the capacity of the resulting channel. It can be observed in Figure 9 that for $n_q = 5$, the high SNR rate is larger than the $n_s \left(1 + \log \left(\frac{n_q - n_s}{n_s}\right)\right)$ lower-bound given in Theorem 4, whereas it is equal to this lower-bound for $n_q = 6$.

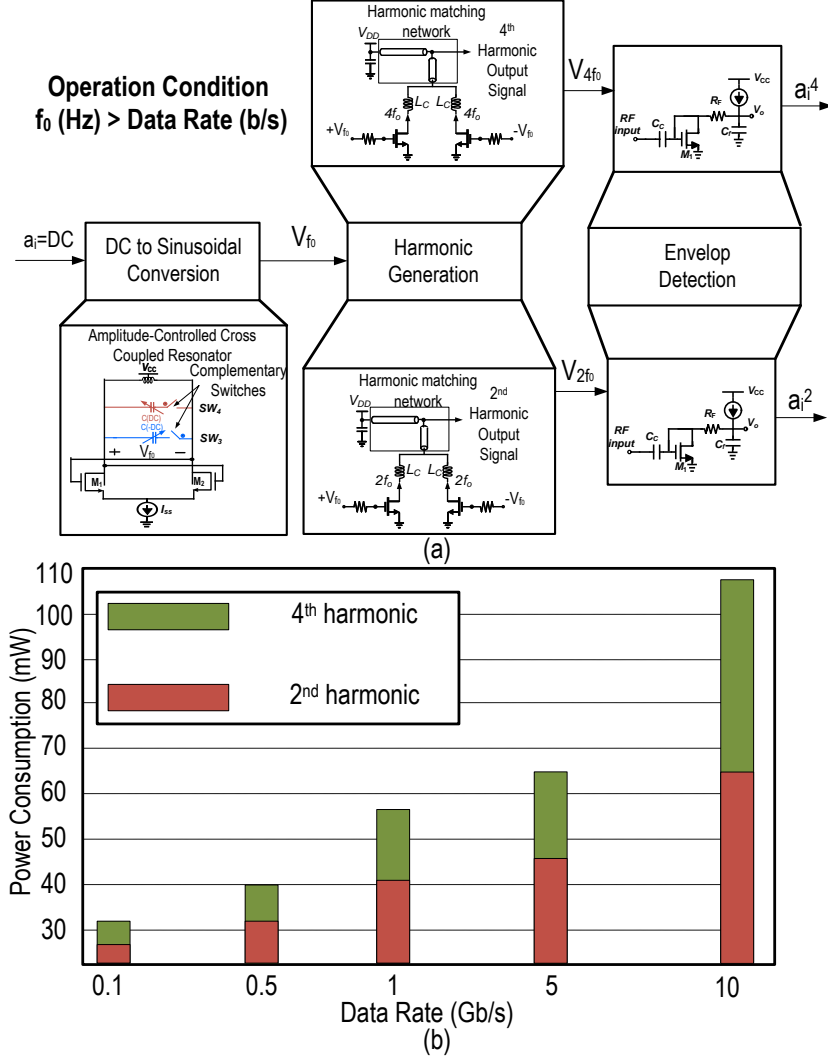


Fig. 8: (a) The circuit design for the generation of fourth and second order polynomials, (b) the power consumption breakdown of the circuits for generation of equal voltage amplitude (corresponding to 0 dBm power) at the second and fourth harmonics.

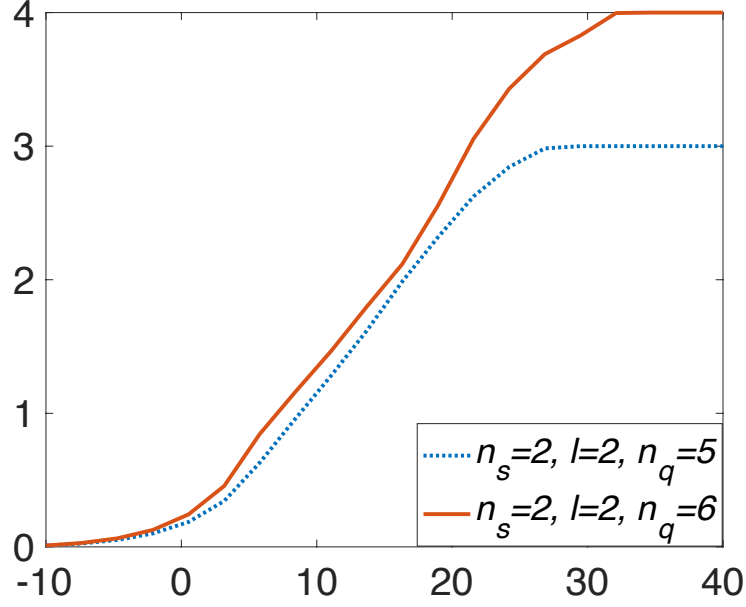


Fig. 9: Inner-bound to achievable rates for the hybrid beamforming architecture of Section IV.

VI. CIRCUIT DESIGN FOR POLYNOMIAL OPERATORS AND ENVELOPE DETECTORS

In this section, we assume that we are given a direct current (DC) signal and our objective is to produce a polynomial function of degree up to four of the input DC value. It can be noted that if the input baseband signal is not a DC value such as a $\text{sinc}(\cdot)$ function, one can use an integrator to transform the signal into a DC value (e.g. [1]). Hence, this assumption does not lose generality.

In practice, there are two methods to achieve the above objective: (i) DC domain nonlinear function synthesis based on the quadratic I-V characteristic of the transistor and increasing the order of polynomial by cascading circuits [50], (ii) translating DC values to sinusoidal waveforms, and then generating harmonics of these waveforms whose amplitude is polynomially dependent on the fundamental frequency amplitude. The former has a simpler circuitry; however it can only be used to produce a specific set of polynomials, i.e., restricted polynomial coefficient values. The latter can produce polynomials with arbitrary coefficients through efficient filtering of undesired harmonic terms. However, it has higher power consumption and more complex circuitry, and its implementation requires careful quantification of the non-linear behavior of transistors, e.g., using Volterra-Weiner series representation methods [7].

To explain the proposed construction, let us consider the problem of producing the fourth order polynomial $f(x) = x^4 + x^2$, where x is the DC input value. Since naturally the amplitude level of the fourth harmonic is less than that of the second harmonic, a harmonic-centric power optimization is needed to produce the desired polynomial. Fig. 8(a) shows a circuit design to generate $f(x) = x^4 + x^2$. In

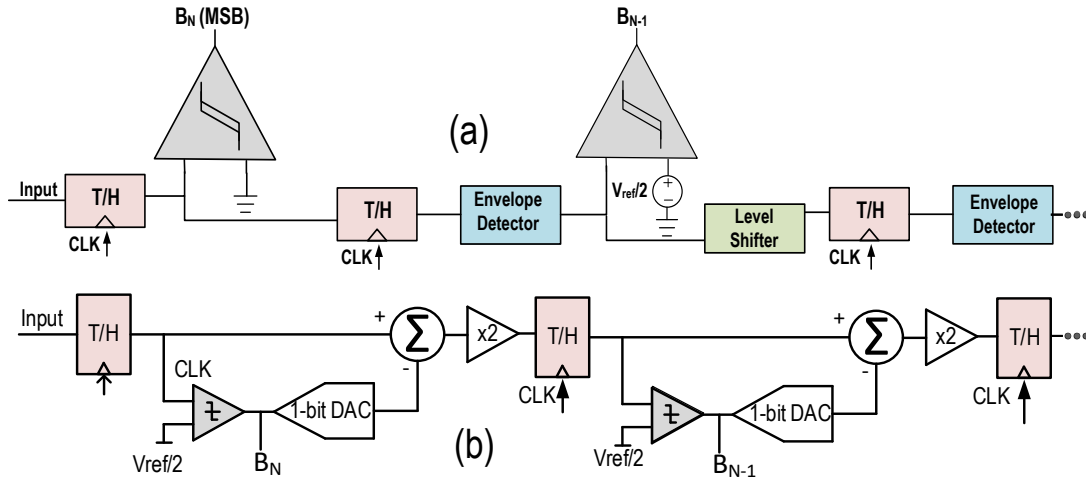


Fig. 10: (a) The cascade of circuits emulating absolute value operators, (b) conventional pipeline ADC architecture.

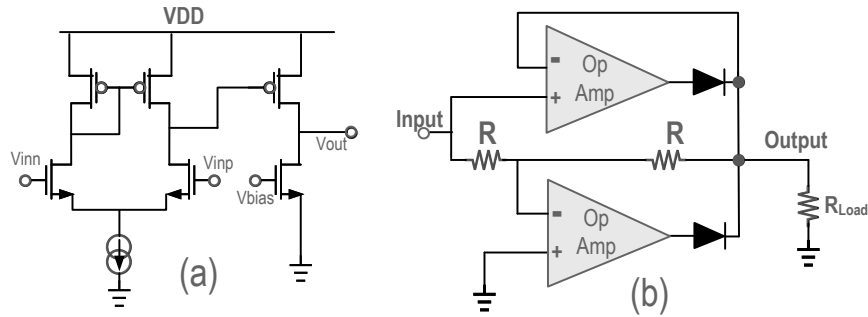


Fig. 11: (a) The deployed differential to single-ended op-amp deployed in the envelope detector (b) the circuit diagram of the implemented envelope detector

order to generate equal amplitudes at the second and fourth harmonics, the power gain of the transistors generating the fourth harmonic should be larger, leading to an increased power consumption in generating the fourth order term compared to the second order term. Figure 8(b) illustrates numerical values for the power consumption of the proposed circuit through simulations. It can be observed that the ratio of the power consumption for the generation of fourth order term compared to the second order term increases with frequency since the transistor power gain drops at higher frequencies. These results are based on CMOS 65nm technology. The power consumption can be further improved by transitioning into smaller transistor nodes.

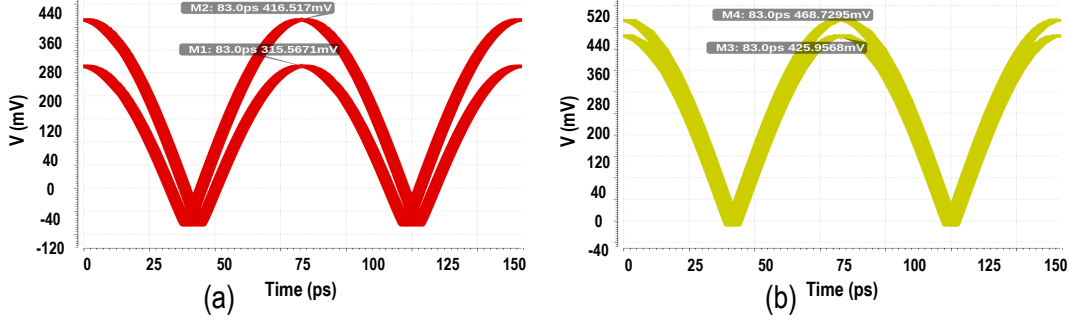


Fig. 12: The impact of amplifier gain on the half-cycle rectification amplitude distortion illustrated for (a) gain of 10 dB, and (b) 25 dB.

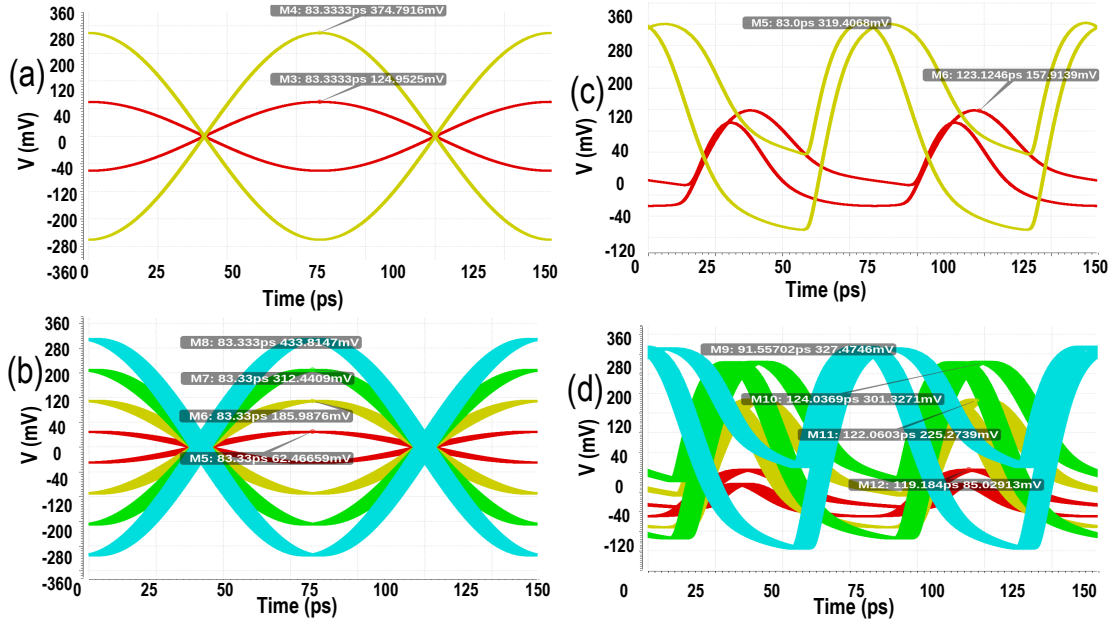


Fig. 13: The input waveform eye diagram for (a) PAM4 and (b) PAM8 modulations compared with the corresponding envelope detector output eye diagrams in (c) and (d).

A. Implementation of Envelop Detectors

In this section, we explain a circuit design for envelope detectors which can be used to realize the receiver architectures studied in prior sections. The circuit block diagram of the proposed multi-step envelope detector is shown in Fig. 10(a). Compared with the conventional pipe-line ADC shown in Fig. 10(b) this circuit exhibits major advantage in terms of power saving by removing the one-bit DAC and subtractor used in each stage. In terms of functionality, the linearity in both scenarios is mainly limited by gain and bandwidth of operational amplifiers (Op-amp) used in functional blocks.

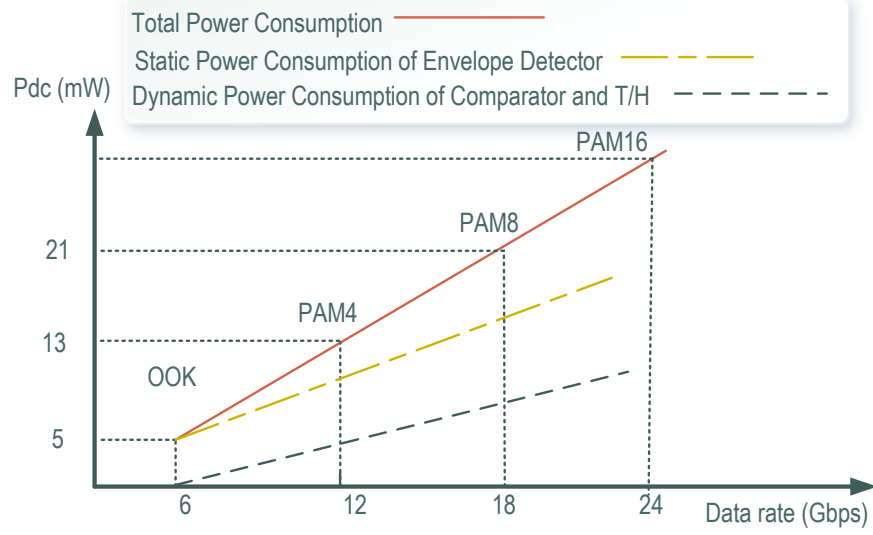


Fig. 14: The linear growth of power consumption with the data rate in envelope detector analog circuits.

The schematic of the envelope detector is shown in Fig. 11. The operational amplifiers deployed in the envelope detector are two stages differential to single-ended amplifiers with gain-bandwidth product (GBW) at 32 GHz in Fig. 11(a). This GBW allows to amplify signals up to 10 GHz with a gain above 15 dB, which is critical for the operation of the envelope detector shown in Fig. 11(b). The resistors in this circuit establish a trade-off between the bandwidth and the waveform distortion. In other words, the larger resistance value leads to smaller distortion of the flipping negative part at the expense of increasing the resistance associated with the output pole of each envelope detector stage, and subsequently limiting the bandwidth of operation. In our simulations, we assumed 500Ω resistors. According to the simulation results shown in Fig. 12, the higher gain of each operational amplifier leads to smaller amplitude distortion at the output, which naturally is achieved at the expense of a smaller bandwidth for the amplifier, thereby leading to a distortion-bandwidth tradeoff. By cascading multiple stages of the envelope detectors, as mentioned in Section II the achievable data-rate increases. To justify this claim, we have simulated the two-stage envelope detector circuit in Fig. 10(a). The DC level shifter is realized by diode-based circuits which consume no DC power and can operate up to desired datarates.

The simulated eye-diagram performance of the two-stage envelope detector is illustrated in Fig. 13. It can be noted that at such higher data rates, in contrast to lower data rates where a square wave is feasible, sinusoidal waveforms are the only feasible inputs to an ADC [51]. Therefore, in our simulations we consider the input to the absolute value function circuitry to be a sinusoidal waveform.

An important characteristic of the envelope detectors is the input dynamic range to support an output

waveform that follows the input amplitude with minimal deviation. By increasing the input magnitude, the amplifier's constituent transistors will be pushed into nonlinear regions of operation, and a "compression behavior" is observed. The point at which this compression happens is an upper-bound on the magnitude of input signals. This value is critical in scenarios where amplitude modulation is deployed in the transceiver. To evaluate our proposed envelope detector, two modulation scenarios of Pulse Amplitude Modulation (PAM)4 and PAM8 modulation schemes are considered as the input to the envelope detector, as shown in Fig. 13. In both cases, the output rectified eye diagram exhibits clear distinction between the amplitude levels (denoted by different colors) such that the comparators in the following one-bit ADCs can distinguish the amplitude levels with small error. The simulation results in Fig. 13 demonstrate that the amplitude ratios at the output follow the input amplitude ratios even when the dynamic range of input waveform is only between -400 to +400 mV. It is also noteworthy that a PAM-8 waveform in the receiver base-band can be constructed by passing the QAM-64 signal (in Table I) through a quadrature down-conversion mixer [52]. By comparing the power consumption of the 2nd and 4th order polynomial analog operations in Fig. 8(b) with the absolute value circuits in Fig. 14, it is clear that the absolute value function lends itself to high-data-rate operations with significantly smaller DC power consumption, which justifies its deployment for THz communication system.

Theorems 2 and 4 show that the channel capacity depends on the number of ADCs through $n_q 2^{\delta_{env}} + 1$ and $n_q \delta_{poly} + 1$, respectively, so that the use of a envelope detectors and quadratic analog operators instead of a linear operators ($\delta_{env} : 0 \rightarrow 1$ and $\delta_{poly} : 1 \rightarrow 2$) has an equivalent effect on capacity as that of quadrupling and doubling the number of ADCs n_q , respectively. This fact, along with the power consumption values given in Figures 14 and 8(b) justify the use of nonlinear analog operators. It should be noted that power consumption is dependent on circuit configuration, transistor size, and passive quality factors. These simulations serve as a proof-of-concept to justify the effectiveness of the proposed receiver architecture designs.

VII. CONCLUSION

The application of nonlinear analog operations in MIMO receivers was considered. A receiver architecture consisting of linear analog combiners, implementable nonlinear analog operators, and few-bit threshold ADCs was designed, and the fundamental information theoretic performance limits of the resulting communication system were investigated. Furthermore, circuit-level simulations, using a 65 nm Bulk CMOS technology, were provided to show the implementability of the desired nonlinear analog operators with practical power budgets.

APPENDIX A

PROOF OF PROPOSITION 6

We provide an outline of the proof. Let us consider the following cases:

Case 1: $\sum_{j=1}^{n_q} \kappa_j \geq 2^{n_q}$

In this case, one can use a balanced Gray code [47] to construct C . A balanced Gray code is a (binary) code where consecutive codewords have Hamming distance equal to one, and each of the bit positions changes value either $2\lfloor \frac{2^{n_q}}{2} \rfloor$ times or $2\lceil \frac{2^{n_q}}{2} \rceil$ times. If $\min_{j \in [n_q]} \kappa_j \geq 2\lceil \frac{2^{n_q}}{2} \rceil$ the proof is complete as one can concatenate the balanced gray code with a series of additional repeated codewords to satisfy the transition counts, and since the balanced gray code is a subcode of the resulting code, we have $|C| = 2^{n_q}$. Otherwise, there exists $j \in [n_q]$ such that $\kappa_j < 2\lceil \frac{2^{n_q}}{2} \rceil$. In this case, without loss of generality, let us assume that $\kappa_1 \leq \kappa_2, \dots \leq \kappa_{n_q}$. Note that since $|\kappa_j - \kappa'_j| \leq 2, j, j' \in [n_q]$ and $\kappa_j, j \in [n_q]$ are even, there is at most one $j^* \in [n_q]$ such that $\kappa_{j^*} \leq \kappa_{j^*+1}$. Let $\kappa'_1, \kappa'_2, \dots, \kappa'_{n_q}$ be the transition count sequence of a balanced gray code C' written in non-decreasing order. Note that $2\lceil \frac{2^{n_q}}{2} \rceil - 2\lfloor \frac{2^{n_q}}{2} \rfloor = 2$. Hence, similar to the above argument, there can only be one $j' \in [n_q]$ for which $\kappa_{j'} \leq \kappa_{j'+1}$. Since $\sum_{j=1}^{n_q} \kappa_j \geq 2^{n_q} = \sum_{j=1}^{n_q} \kappa'_j$, we must have $j^* \leq j'$. So, the balanced gray code can be used as a subcode similar to the previous case by correctly ordering the bit positions to match the order of $\kappa_j, j \in [n_q]$. This completes the proof.

Case 2: $\sum_{j=1}^{n_q} \kappa_j < 2^{n_q}$

The proof is based on techniques used in the construction of balanced Gray codes [47]. We prove the result by induction on n_q . The proof for $n_q = 1, 2$ is straightforward and follows by construction of length-one and length-two sequences. For $n_q > 2$, Assume that the result holds for all $n'_q \leq n_q$. Without loss of generality, assume that $\kappa_1 \leq \kappa_2 \leq \dots \leq \kappa_{n_q}$. The proof considers four sub-cases as follows.

Case 2.i: $\sum_{j=3}^{n_q} \kappa_j \in [0, 2^{n_q-2}]$

In this case, by the induction assumption, there exists C' , a code with codewords of length $n_q - 2$, whose transition sequence is $\kappa_3, \kappa_4, \dots, \kappa_{n_q}$, and $|C'| = \sum_{j=3}^{n_q} \kappa_j$. We construct C from C' as follows. Let $\mathbf{c}_0 = (0, 0, \mathbf{c}'_0)$, $\mathbf{c}_1 = (0, 1, \mathbf{c}'_0)$, $\mathbf{c}_2 = (1, 1, \mathbf{c}'_0)$, $\mathbf{c}_3 = (1, 0, \mathbf{c}'_0)$, $\mathbf{c}_4 = (1, 0, \mathbf{c}'_1)$, $\mathbf{c}_5 = (0, 0, \mathbf{c}'_1)$, $\mathbf{c}_6 = (0, 1, \mathbf{c}'_1)$, $\mathbf{c}_7 = (1, 1, \mathbf{c}'_1), \dots$. This resembles the procedure for constructing balanced gray codes [47]. We continue concatenating the first two bits of each codeword in C to the codewords in C' using the procedure described above until κ_1 transitions for position 1 and κ_2 transitions for position 2 have taken place. Note that this is always possible since i) for each two codewords in C' , we ‘spend’ two transitions of each of the first and second positions in C to produce four new codewords, ii) $\kappa_2 - \kappa_1 \leq 2$, and iii) $\kappa_2 \leq \sum_{j=3}^{n_q} \kappa_j$, where the latter condition ensures that we do not run out of codewords in C' before the necessary transitions in positions 1 and 2 are completed. After $\kappa_2 + 1$ codewords, the transitions in positions 1 and 2 are

completed, and the last produced codeword is $(0, 0, \mathbf{c}'_{\kappa_2+1})$ since κ_1 and κ_2 are both even. To complete the code C , we add $(0, 0, \mathbf{c}'_i), i \in [\kappa_2 + 2, \sum_{j=3}^{n_q} \kappa_j]$. Then, by construction, we have $|C| = |C'| + \kappa_1 + \kappa_2 = \sum_{j=1}^{n_q} \kappa_j$ and the code satisfied Properties 1), 2), 3), and 5) in Proposition 4.

Case 2.ii: $\sum_{j=3}^{n_q} \kappa_j \in [2^{n_q-2}, 2^{n_q-1}]$

Similar to the previous case, let C' be a balanced gray code with codeword length $n_q - 2$ and transition counts $\kappa'_1 \leq \kappa'_2 \leq \dots \leq \kappa'_{n_q-2}$. Define $\kappa''_j = \kappa_j - \kappa'_{j+2}, j \in \{3, 4, \dots, n_q\}$. Note that κ''_j satisfy the conditions on transition counts in the proposition statement, and hence by the induction assumption, there exists a code C'' with transition counts $\kappa''_j, j \in [n_q - 2]$. The proof is completed by appropriately concatenating C' and C'' to construct C . Let γ'' be the number of codewords in C'' and define $\mathbf{c}_i = (0, 0, \mathbf{c}''_i), i \in [\gamma'']$, $\mathbf{c}_{\gamma''+1} = (0, 1, \mathbf{c}''_{\gamma''})$, $\mathbf{c}_{\gamma''+2} = (1, 1, \mathbf{c}''_{\gamma''})$, $\mathbf{c}_{\gamma''+3} = (1, 0, \mathbf{c}''_{\gamma''})$, $\mathbf{c}_{\gamma''+4} = (1, 0, \mathbf{c}'_1), \dots$. Similar to the previous case, it is straightforward to show that this procedure yields a code C with the desired transition sequence.

The proof for the two subcases where $\sum_{j=3}^{n_q} \kappa_j \in [2^{n_q-1}, 3 \times 2^{n_q-2}]$ and $\sum_{j=3}^{n_q} \kappa_j \in [3 \times 2^{n_q-1}, 2^{n_q}]$ is similar and is omitted for brevity.

REFERENCES

- [1] Farhad Shirani and Hamidreza Aghasi. Mimo systems with one-bit adcs: Capacity gains using nonlinear analog operations. In *2022 IEEE International Symposium on Information Theory (ISIT)*, pages 2511–2516, 2022.
- [2] Farhad Shirani and Hamidreza Aghasi. Quantifying the capacity gains in coarsely quantized siso systems with nonlinear analog operators. *arXiv preprint arXiv:2208.04450*, 2022.
- [3] Ahmed M Al-samman, Marwan Hadri Azmi, and Tharek Abd Rahman. A survey of millimeter wave (mm-wave) communications for 5g: Channel measurement below and above 6 ghz. In *International Conference of Reliable Information and Communication Technology*, pages 451–463. Springer, 2018.
- [4] Hadi Sarieddeen, Mohamed-Slim Alouini, and Tareq Y Al-Naffouri. An overview of signal processing techniques for terahertz communications. *Proceedings of the IEEE*, 2021.
- [5] Christina Chaccour, Mehdi Naderi Soorki, Walid Saad, Mehdi Bennis, Petar Popovski, and M  rouane Debbah. Seven defining features of terahertz (thz) wireless systems: A fellowship of communication and sensing. *IEEE Communications Surveys & Tutorials*, 24(2):967–993, 2022.
- [6] Heedong Do, Sungmin Cho, Jeonghun Park, Ho-Jin Song, Namyoon Lee, and Angel Lozano. Terahertz line-of-sight mimo communication: Theory and practical challenges. *IEEE Communications Magazine*, 59(3):104–109, 2021.
- [7] Hamidreza Aghasi, Andreia Cathelin, and Ehsan Afshari. A 0.92-thz sige power radiator based on a nonlinear theory for harmonic generation. *IEEE Journal of Solid-State Circuits*, 52(2):406–422, 2017.
- [8] Zhi Hu, Mehmet Kaynak, and Ruonan Han. High-power radiation at 1 thz in silicon: A fully scalable array using a multi-functional radiating mesh structure. *IEEE Journal of Solid-State Circuits*, 53(5):1313–1327, 2018.
- [9] Peyman Nazari, Saman Jafarlou, and Payam Heydari. A cmos two-element 170-ghz fundamental-frequency transmitter with direct rf-8psk modulation. *IEEE Journal of Solid-State Circuits*, 55(2):282–297, 2019.
- [10] Shinwon Kang, Siva V Thyagarajan, and Ali M Niknejad. A 240 ghz fully integrated wideband qpsk transmitter in 65 nm cmos. *IEEE Journal of Solid-State Circuits*, 50(10):2256–2267, 2015.

- [11] Kaushik Sengupta, Dongjin Seo, Lita Yang, and Ali Hajimiri. Silicon integrated 280 ghz imaging chipset with 4times 4 sige receiver array and cmos source. *IEEE Transactions on Terahertz Science and Technology*, 5(3):427–437, 2015.
- [12] Md Hedayatullah Maktoomi, Zisong Wang, Huan Wang, Soheil Saadat, Payam Heydari, and Hamidreza Aghasi. A sub-terahertz wideband stacked-patch antenna on a flexible printed circuit for 6g applications. *IEEE Transactions on Antennas and Propagation*, 70(11):10047–10061, 2022.
- [13] Boris Murmann et al. Adc performance survey 1997-2016, 2018.
- [14] Behzad Razavi. *Principles of data conversion system design*, volume 126. IEEE press New York, 1995.
- [15] Boris Murmann. The race for the extra decibel: a brief review of current ADC performance trajectories. *IEEE Solid-State Circuits Magazine*, 7(3):58–66, 2015.
- [16] Jiayi Zhang, Linglong Dai, Xu Li, Ying Liu, and Lajos Hanzo. On low-resolution adcs in practical 5g millimeter-wave massive mimo systems. *IEEE Communications Magazine*, 56(7):205–211, 2018.
- [17] Theodore S Rappaport, Robert W Heath Jr, Robert C Daniels, and James N Murdock. *Millimeter wave wireless communications*. Pearson Education, 2015.
- [18] Wonbin Hong, Kwang-Hyun Baek, Youngju Lee, Yoongeon Kim, and Seung-Tae Ko. Study and prototyping of practically large-scale mmwave antenna systems for 5G cellular devices. *IEEE Communications Magazine*, 52(9):63–69, 2014.
- [19] Kamal Sarabandi, Armin Jam, Mehrnoosh Vahidpour, and Jack East. A novel frequency beam-steering antenna array for submillimeter-wave applications. *IEEE Transactions on Terahertz Science and Technology*, 8(6):654–665, 2018.
- [20] Boyu Ning, Zhongbao Tian, Zhi Chen, Chong Han, Jinhong Yuan, and Shaoqian Li. Prospective beamforming technologies for ultra-massive mimo in terahertz communications: A tutorial. *arXiv preprint arXiv:2107.03032*, 2021.
- [21] Shuangfeng Han, I Chih-Lin, Zhikun Xu, and Corbett Rowell. Large-scale antenna systems with hybrid analog and digital beamforming for millimeter wave 5G. *IEEE Communications Magazine*, 53(1):186–194, 2015.
- [22] Robert W Heath, Nuria Gonzalez-Prelcic, Sundeep Rangan, Wonil Roh, and Akbar M Sayeed. An overview of signal processing techniques for millimeter wave MIMO systems. *IEEE journal of selected topics in signal processing*, 10(3):436–453, 2016.
- [23] Roi Méndez-Rial, Cristian Rusu, Ahmed Alkhateeb, Nuria González-Prelcic, and Robert W Heath. Channel estimation and hybrid combining for mmwave: Phase shifters or switches? In *2015 Information Theory and Applications Workshop (ITA)*, pages 90–97. IEEE, 2015.
- [24] Robert H Walden. Analog-to-digital converter survey and analysis. *IEEE Journal on selected areas in communications*, 17(4):539–550, 1999.
- [25] Hang Yuan, Nan Yang, Kai Yang, Chong Han, and Jianping An. Hybrid beamforming for terahertz multi-carrier systems over frequency selective fading. *IEEE Transactions on Communications*, 68(10):6186–6199, 2020.
- [26] Chong Han, Longfei Yan, and Jinhong Yuan. Hybrid beamforming for terahertz wireless communications: Challenges, architectures, and open problems. *IEEE Wireless Communications*, 28(4):198–204, 2021.
- [27] Andreas F Molisch, Vishnu V Ratnam, Shengqian Han, Zheda Li, Sinh Le Hong Nguyen, Linsheng Li, and Katsuyuki Haneda. Hybrid beamforming for massive MIMO: A survey. *IEEE Communications Magazine*, 55(9):134–141, 2017.
- [28] Ahmed Alkhateeb, Jianhua Mo, Nuria Gonzalez-Prelcic, and Robert W Heath. MIMO precoding and combining solutions for millimeter-wave systems. *IEEE Communications Magazine*, 52(12):122–131, 2014.
- [29] A. Khalili, S. Rini, L. Barletta, E. Erkip, and Y. C. Eldar. On MIMO channel capacity with output quantization constraints. In *2018 IEEE International Symposium on Information Theory (ISIT)*, pages 1355–1359, June 2018.
- [30] Abbas Khalili, Shahram Shahsavari, Farhad Shirani, Elza Erkip, and Yonina C Eldar. On throughput of millimeter wave

- MIMO systems with low resolution ADCs. In *ICASSP 2020-2020 IEEE International Conference on Acoustics, Speech and Signal Processing (ICASSP)*, pages 5255–5259. IEEE, 2020.
- [31] Sourjya Dutta, Abbas Khalili, Elza Erkip, and Sundeeep Rangan. Capacity bounds for communication systems with quantization and spectral constraints. In *2020 IEEE International Symposium on Information Theory (ISIT)*, pages 2038–2043. IEEE, 2020.
 - [32] Christopher Mollén, Junil Choi, Erik G Larsson, and Robert W Heath. Achievable uplink rates for massive mimo with coarse quantization. In *2017 IEEE International Conference on Acoustics, Speech and Signal Processing (ICASSP)*, pages 6488–6492. IEEE, 2017.
 - [33] Christopher Mollen, Junil Choi, Erik G Larsson, and Robert W Heath. One-bit adcs in wideband massive mimo systems with ofdm transmission. In *2016 IEEE International Conference on Acoustics, Speech and Signal Processing (ICASSP)*, pages 3386–3390. IEEE, 2016.
 - [34] Sven Jacobsson, Giuseppe Durisi, Mikael Coldrey, Ulf Gustavsson, and Christoph Studer. Throughput analysis of massive mimo uplink with low-resolution adcs. *IEEE Transactions on Wireless Communications*, 16(6):4038–4051, 2017.
 - [35] Hessam Pirzadeh and A Lee Swindlehurst. Spectral efficiency of mixed-adc massive mimo. *IEEE Transactions on Signal Processing*, 66(13):3599–3613, 2018.
 - [36] Yongzhi Li, Cheng Tao, Gonzalo Seco-Granados, Amine Mezghani, A Lee Swindlehurst, and Liu Liu. Channel estimation and performance analysis of one-bit massive mimo systems. *IEEE Transactions on Signal Processing*, 65(15):4075–4089, 2017.
 - [37] Steven Callender, Abhishek Agrawal, Amy Whitcombe, Ritesh Bhat, Mustafijur Rahman, Chun C Lee, Peter Sagazio, Georgios C Dogiamis, Brent R Carlton, Christopher Hull, et al. A fully integrated 160-gb/s d-band transmitter achieving 1.1-pj/b efficiency in 22-nm finfet. *IEEE Journal of Solid-State Circuits*, 2022.
 - [38] Jingbo Tan and Linglong Dai. Thz precoding for 6g: Applications, challenges, solutions, and opportunities. *arXiv preprint arXiv:2005.10752*, 2020.
 - [39] Thomas Kleine-Ostmann and Tadao Nagatsuma. A review on terahertz communications research. *Journal of Infrared, Millimeter, and Terahertz Waves*, 32(2):143–171, 2011.
 - [40] Zihao Zheng, Lai Wei, Jorge Lagos, Ewout Martens, Yan Zhu, Chi-Hang Chan, Jan Craninckx, and Rui P Martins. 16.3 a single-channel 5.5 mw 3.3 gs/s 6b fully dynamic pipelined adc with post-amplification residue generation. In *2020 IEEE International Solid-State Circuits Conference-(ISSCC)*, pages 254–256. IEEE, 2020.
 - [41] Abbas Khalili, Farhad Shirani, Elza Erkip, and Yonina C Eldar. MIMO networks with one-bit ADCs: Receiver design and communication strategies. *IEEE Transactions on Communications*, 2021.
 - [42] Abbas Khalili, Stefano Rini, Luca Barletta, Elza Erkip, and Yonina C Eldar. On MIMO channel capacity with output quantization constraints. In *2018 IEEE International Symposium on Information Theory (ISIT)*, pages 1355–1359. IEEE, 2018.
 - [43] Jaspreet Singh, Onkar Dabeer, and Upamanyu Madhow. On the limits of communication with low-precision analog-to-digital conversion at the receiver. *IEEE Trans. on Communications*, 57(12):3629–3639, 2009.
 - [44] Hans S. Witsenhausen. Some aspects of convexity useful in information theory. *IEEE Transactions on Information Theory*, 26(3):265–271, 1980.
 - [45] Jianyi Huang and Sean P Meyn. Characterization and computation of optimal distributions for channel coding. *IEEE Transactions on Information Theory*, 51(7):2336–2351, 2005.
 - [46] Mari Kobayashi, Giuseppe Caire, and Gerhard Kramer. Joint state sensing and communication: Optimal tradeoff for a memoryless case. In *2018 IEEE International Symposium on Information Theory (ISIT)*, pages 111–115. IEEE, 2018.

- [47] Girish S Bhat and Carla D Savage. Balanced gray codes. *the electronic journal of combinatorics*, 3(1):R25, 1996.
- [48] Igor Sergeevich Bykov. On locally balanced gray codes. *Journal of Applied and Industrial Mathematics*, 10(1):78–85, 2016.
- [49] Gerald L Alexanderson and John E Wetzel. Simple partitions of space. *Mathematics magazine*, 51(4):220–225, 1978.
- [50] Suraj Sindia, Virendra Singh, and Vishwani D Agrawal. Polynomial coefficient based dc testing of non-linear analog circuits. In *Proceedings of the 19th ACM Great Lakes symposium on VLSI*, pages 69–74, 2009.
- [51] Jafar Savoj, Kenny Hsieh, Parag Upadhyaya, Fu-Tai An, Jay Im, Xuewen Jiang, Jalil Kamali, Kang Wei Lai, Daniel Wu, Elad Alon, and Ken Chang. Design of high-speed wireline transceivers for backplane communications in 28nm cmos. In *Proceedings of the IEEE 2012 Custom Integrated Circuits Conference*, pages 1–4, 2012.
- [52] Behzad Razavi and Razavi Behzad. *RF microelectronics*, volume 2. Prentice hall New York, 2012.